Ocean Engineering 111 (2016) 179–197

Contents lists available at ScienceDirect

Ocean Engineering

journal homepage: www.elsevier.com/locate/oceaneng

Hydrodynamic analysis of an array of interacting free-floating oscillating water column (OWC's) devices

D.N. Konispoliatis, S.A. Mavrakos *

Laboratory for Floating Structures and Mooring Systems, Division of Marine Structures, School of Naval Architecture and Marine Engineering, National Technical University of Athens, 9 Heroon Polytechniou Avenue, GR 157-73 Athens, Greece

ARTICLE INFO

Article history:
Received 30 May 2015
Accepted 20 October 2015

Keywords:
Wave power
OWC array
Hydrodynamic analysis
Power efficiency
Wave forces
Motions

ABSTRACT

The paper deals with the hydrodynamic analysis of an array of oscillating water column (OWC) devices that is floating independently in finite depth waters and exposed to the action of regular surface waves. Linearized potential flow theory is assumed. Numerical results are given from the analytical solution of three boundary value problems, namely, the diffraction, the motion – and the pressure-dependent radiation problems. In all cases the interaction phenomena with neighboring bodies have been taken properly into account. First and mean second order wave forces, added masses and damping coefficients, together with air volume flow rates and wave power efficiency from each device are parametrically evaluated.

1. Introduction

Renewable energy technology is steadily gaining importance in the world energy market due to the limited nature of fossil fuel supplies, national requirements for security of supply, as well as political pressure toward the reduction of carbon emissions. The ability of converting wave energy into usable energy has inspired numerous inventors: more than 1000 patents had been registered by 1980 (McCormick, 1980) and the number has increased since then (Falcao, 2010). Among several classes of designs proposed for the wave energy conversion the oscillating water column device (OWC) has received considerable theoretical attention (Evans, 1982; Sarmento et al., 1990; Evans and Porter, 1996; Falnes, 2002; Martins–Rivas and Mei, 2009a). A number of different designs of such wave energy devices have been presented in the literature, the most of them being single devices installed onshore (Falcao, 2010), whereas lately there are some designs of free floating or moored devices in the open sea (Mavrakos and Konispoliatis, 2012).

As far as the case of an array of those devices is concerned, the research has mostly been concentrated to restrained OWC's wave energy converters (WEC). In this context, theoretical studies have been presented by Falcao (2002); Nihous (2012) and Nader et al. (2012, 2014), and experimental ones by Aubault et al. (2011) and Bryden and Linfoot (2010). Considering the case of arrays of free-floating wave energy converters, the so-called WEC farms, theoretical studies have been developed in the literature for capturing the hydrodynamic interaction effects among the devices. This aspect has been covered by Babarit et al. (2010); Borgarino et al. (2012); Babarit (2013) and Singh and Babarit (2014) in regular and irregular wave fields. Moreover, Child and Venugopal (2010) and Child et al. (2011) presented a numerical optimization scheme for obtaining array layouts with the most favorable total power absorption levels at a particular wave number and direction, while Folley et al. (2012) made a snap-shot of the currently available numerical modelling techniques for WEC.

The main difference between an isolated OWC device and an array of such devices is the hydrodynamic interaction phenomena between the array's members. Each device of the configuration scatters waves towards the others, which in turn scatter waves contributing to the excitation of the initial device and so on. In the present contribution, the total wave field around each body of the multi-body configuration is obtained by superposing the incident wave potential and various orders of successively reflected waves emanating from all the devices of the arrangement using the physical idea of multiple scattering that has been introduced by Twersky (1952) in studying the acoustic scattering by an array of parallel cylinders. This idea was applied to free-surface body–wave interaction problems by Ohkusu (1974) for the case of three adjacent, floating, vertical truncated cylinders. The method was then extended by Mavrakos and Koumoutsakos (1987) and Mavrakos (1991) for the solution of the diffraction and radiation problems by an array of arbitrarily shaped vertical axisymmetric bodies with any geometrical arrangement and individual bodies'

* Corresponding author. Tel.: +30 210 7721121.
E-mail address: mavrakos@naval.ntua.gr (S.A. Mavrakos).

http://dx.doi.org/10.1016/j.oceaneng.2015.10.034
0029-8018/

geometries. Mavrakos (1996) solved the diffraction problem by an array of bottomless vertical axisymmetric bodies, with finite wall thickness while Mavrakos and McIver (1997) compared the results obtained by the multiple scattering formulation with the plane-wave approximation and computed the wave forces, hydrodynamic coefficients and the gain q–factors of a finite array of wave power devices.

Besides the multiple scattering approaches, direct matrix inversion methods have been presented in the literature as well to solve the hydrodynamic interaction problem among arrays of bodies for which the diffraction solution is known (Kagemoto and Yue, 1986). This method has been also used by Siddorn and Eatock Taylor (2008) in order to elaborate an exact algebraic method for the diffraction and independent radiation by an array of truncated cylinders.

In the present contribution an array of multiple interacting vertical axisymmetric oscillating water column devices is investigated, exposed to the action of regular surface waves in finite water depth. The devices have finite wall thickness and are floating independently. Numerical results are given from the solution of three boundary value problems, namely, the diffraction problem-each body is fixed in waves, atmospheric pressure in each OWC–, the motion-dependent radiation problem resulting from the forced oscillations of each body in otherwise still water, also under atmospheric conditions above each OWC, and the pressure-dependent radiation problem resulting from an oscillating pressure head acting on the inner free surface of each OWC. Particularly, numerically evaluated linear exciting wave forces along with the volume flow, the added mass and wave damping coefficients are calculated for each freely floating device. In addition, the mean second order loads acting on each OWC device are presented. In view of evaluating the rigid body motions of each device, the motion equations are solved in the frequency domain, for various values of turbine parameters related to the pressure drop inside each oscillating chamber. Final, the power efficiency over a range of wave frequencies from each device of the array for various spacing among the OWC's is being calculated.

2. Description of the hydrodynamic problem

2.1. Governing equations and single-body velocity potential representations

We consider a group of N floating vertical axisymmetric oscillating water column devices that is excited by a plane periodic wave of amplitude $H/2$, frequency ω and wave number k propagating in water of finite water depth d. The outer and inner radii of each device's chamber q, $q=1, 2,\ldots, N$, are denoted by a_q, b_q, respectively, whereas the distance between the bottom of the q device and the sea bed is denoted by h_q, as illustrated in Fig. 1. The fluid is assumed non viscous and incompressible and the flow irrotational, so that linear potential theory can be employed. A global Cartesian co-ordinate system O–XYZ with origin on the sea bed and its vertical axis OZ directed positive upwards is used. Moreover, N local cylindrical co-ordinate systems (r_q, θ_q, z_q), $q=1, 2,\ldots, N$ are defined with origins on the sea bottom and their vertical axes pointing upwards and coinciding with the vertical axis of symmetry of the q device.

The fluid flow around each of the $q=1,2,\ldots,N$ device can be described by the potential function:

$$\Phi^q(r_q,\theta_q,z;t)=\mathrm{Re}\left\{\phi^q(r_q,\theta_q,z)\cdot e^{-i\omega t}\right\} \tag{2.1}$$

Following Falnes and McIver (1985) the spatial function ϕ^q can be decomposed, on the basis of linear modeling, as:

$$\phi^q=\phi_0^q+\phi_7^q+\sum_{p=1}^{N}\sum_{j=1}^{6}\dot{\xi}_{j0}^p\cdot\phi_j^{qp}+\sum_{p=1}^{N}p_{in0}^p\cdot\phi_P^{qp} \tag{2.2}$$

Here, ϕ_0^q is the velocity potential of the undisturbed incident harmonic wave; ϕ_7^q is the scattered potential around the q device, when it is considered fixed in waves with the duct open to the atmosphere, so that the pressure in the chamber is equal to the atmospheric one; ϕ_j^{qp} is the motion-dependent radiation potential around the body q resulting from the forced oscillation of the p body in j direction with unit velocity amplitude, $\dot{\xi}_{j0}^p$, $(j=1, 2,\ldots,6)$, the air chambers of both p and q devices being considered open to the atmosphere.

It holds $\xi_j^p=\mathrm{Re}\left\{\dot{\xi}_{j0}^p\cdot e^{-i\omega t}\right\}=\mathrm{Re}\left\{-i\omega\xi_{j0}^p\cdot e^{-i\omega t}\right\}$ and the subscript j stands for surge $(j=1)$, sway $(j=2)$, heave $(j=3)$, roll $(j=4)$, pitch $(j=5)$ and yaw $(j=6)$ modes of motions, respectively. Moreover, ϕ_P^{qp} is the pressure-dependent radiation potential around the q body when it is considered fixed in the wave field and open to the atmosphere due to unit time harmonic oscillating pressure head, $P_{in}^p=\mathrm{Re}\{p_{in0}^p\cdot e^{-i\omega t}\}$, in the chamber of the p device which is considered fixed in otherwise calm water.

The potentials ϕ_j^q $(j=0, 7; q=1, 2, \ldots, N)$, ϕ_j^{qp} $(j=1, \ldots, 6; p, q=1, 2,\ldots, N)$ and ϕ_P^{qp} $(p, q=1, 2,\ldots, N)$ are solutions of Laplace's equation in the entire fluid domain and satisfy the zero normal velocity on the sea bed $(z=0)$ and the following boundary conditions on the

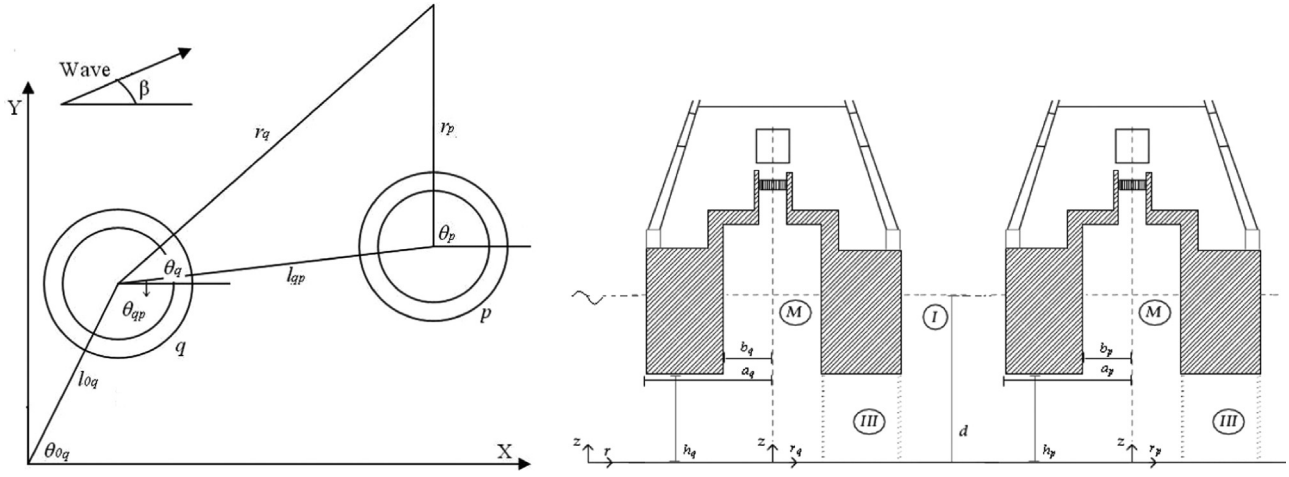

Fig. 1. Definition sketch of the q OWC device of the array.

outer and inner free sea surface ($z=d$) of each body:

$$\omega^2\phi_j^q - g\frac{\partial\phi_j^q}{\partial z}=0 \text{ for } r_q\geq a_q;\ 0\leq r_q\leq b_q,\ j=0,7 \tag{2.3}$$

$$\omega^2\phi_j^{qp} - g\frac{\partial\phi_j^{qp}}{\partial z}=0 \text{ for } r_q\geq a_q;\ 0\leq r_q\leq b_q,\ j=1,2,...,6 \tag{2.4}$$

$$\omega^2\phi_P^{qp} - g\frac{\partial\phi_P^{qp}}{\partial z}=\left\{\begin{array}{cc} 0 & \text{for } r_q\geq a_q \\ -\delta_{q,p}\frac{i\omega}{\rho} & \text{for } 0\leq r_q\leq b_q\end{array}\right\} \tag{2.5}$$

Furthermore, the potentials have to fulfill following kinematic conditions on the mean body's wetted surface:

$$\frac{\partial\phi_7^q}{\partial\vec{n}^q}=-\frac{\partial\phi_0^q}{\partial\vec{n}^q} \tag{2.6}$$

$$\frac{\partial\phi_P^{qp}}{\partial\vec{n}^q}=0 \tag{2.7}$$

$$\frac{\partial\phi_j^{qp}}{\partial\vec{n}^q}=\delta_{q,p}n_j^p, j\equiv 1,...,6 \tag{2.8}$$

Here $\partial(\ )/\partial\vec{n}^q$ denotes the derivative in the direction of the outward unit normal vector $\vec{n}^q$, to the mean wetted surface S_0^q on the q–th body, and n_j^p, are its generalized components defined as $\vec{n}^p=(n_1^p,n_2^p,n_3^p)$ and $\vec{r}^p\times\vec{n}^p=(n_4^p,n_5^p,n_6^p)$, where $\vec{r}^p$ is the position vector with respect to the origin of the coordinate system. Finally, a radiation condition must be imposed which states that propagating disturbances must be outgoing.

The velocity potential of the undisturbed incident wave,ϕ_0^q, propagating at angle β, (Fig. 1), with respect to the positive x–axis can be expressed in the cylindrical co-ordinate frame of the q-th body as follows (Mavrakos and Koumoutsakos, 1987):

$$\phi_0^q(r_q,\theta_q,z)=-i\omega\frac{H}{2}\sum_{m=-\infty}^{\infty} i^m\Psi_{0,m}^q(r_q,z)\cdot e^{im\theta_q} \tag{2.9}$$

where

$$\frac{1}{d}\Psi_{0,m}^q(r_q,z)=e^{ik\ell_{oq}\cos(\theta_{oq}-\beta)}\frac{Z_0(z)}{d\cdot Z_0'(d)}J_m(kr_q)\cdot e^{-im\beta} \tag{2.10}$$

The symbols used above are defined in Fig. 1. Here J_m is the m-th order Bessel function of first kind and $Z_0(z)$ is defined by:

$$Z_0(z)=\left[\frac{1}{2}\cdot\left[1+\frac{\sinh(2kd)}{2kd}\right]\right]^{-1/2}\cdot\cosh(kz) \tag{2.11}$$

with $Z_0'(d)$ being its derivative at $z=d$. Frequency ω and wave number k are related by the dispersion equation.

In accordance to (2.9), the diffraction, i.e.$\phi_D^q=\phi_0^q+\phi_7^q$, the motion–, and pressure-dependent radiation potentials around the q device, when it is considered alone in the wave field, can be expressed in its own cylindrical co-ordinate system (r_q,θ_q,z) as follows:

$$\phi_D^q(r_q,\theta_q,z)=-i\omega\frac{H}{2}\sum_{m=-\infty}^{\infty} i^m\Psi_{D,m}^q(r_q,z)\cdot e^{im\theta_q} \tag{2.12}$$

$$\phi_j^q(r_q,\theta_q,z)=-i\omega\sum_{m=-\infty}^{\infty}\Psi_{j,m}^q(r_q,z)\cdot e^{im\theta_q} \tag{2.13}$$

$$\phi_P^q(r_q,\theta_q,z)=\frac{1}{i\omega\rho}\sum_{m=-\infty}^{\infty}\Psi_{P,m}^q(r_q,z)\cdot e^{im\theta_q} \tag{2.14}$$

here ρ is the water density. The unknown potential functions $\Psi_{D,m}^q,\Psi_{j,m}^q$, and $\Psi_{P,m}^q$ involved in Eqs. (2.12)–(2.14) can be established through the method of matched axisymmetric eigenfunction expansions. In doing so, the flow field around the device q is subdivided in coaxial ring-shaped fluid regions, categorized by the numerals *I, III* and *M* (Fig. 1). In each of those regions, different series expansions of the velocity potentials $\Psi_{D,m}^{k,q},\Psi_{j,m}^{k,q}$, and $\Psi_{P,m}^{k,q}$ (k=*I, III,* and M) can be made.

These are solutions of the Laplace equation in each fluid region and are selected in such a way that the kinematic boundary condition at the horizontal walls of the cylindrical OWC device, the linearized condition on the free surface, the kinematic condition on the sea bottom and the radiation condition at infinity are *a priori* satisfied. The various potential solutions are then matched by continuity requirements of the hydrodynamic pressure and radial velocity along the vertical boundaries of adjacent fluid regions, as well as by fulfilling the kinematic conditions at the vertical walls of the body. This procedure delivers the linear systems of equations for the determination of the unknown coefficients needed for the series representations of the velocity potential in each fluid region. The method has been extensively described in the past (see for example the works by Miles and Gilbert (1968), Garrett (1971), Black et al. (1971), Yeung (1981), Mei (1983) as far as a circular dock is concerned; by Mavrakos (1985, 1988) for bottomless cylinders; by Mavrakos and Konispoliatis (2012) for single OWC's devices with finite wall thickness and by Kokkinowrachos et al. (1987) for the hydrodynamic analysis of arbitrary shaped vertical bodies of revolution). It is therefore no further elaborated here.

In the outer fluid domain *I* of the body q, i.e. for $r_q\geq a_q$, $0\leq z\leq d$, when the body q is considered alone in the wave field, the appropriate series representations of the potential functions $\Psi_{j,m}^{I,q}$ involved in (2.12)–(2.14) for the diffraction ($j=D$), the motion-radiation (j=1, 3, and 5) and the pressure-radiation ($j=P$) problems are:

$$\frac{1}{\delta_j}\Psi_{j,m}^{I,q}(r_q,z)=g_{j,m}^{I,q}(r_q,z)+\sum_{n=0}^{\infty}F_{j,mn}^{I,q}\frac{K_m(a_nr_q)}{K_m(a_na_q)}Z_n(z) \tag{2.15}$$

where

$$g_{D,m}^{I,q}(r_q,z)=\left\{J_m(kr_q)-\frac{J_m(ka_q)}{H_m(ka_q)}H_m(kr_q)\right\}\frac{Z_0(z)}{d.Z_0'(d)}$$
$$g_{1,1}^{I,q}(r_q,z)=g_{3,0}^{I,q}(r_q,z)=g_{5,1}^{I,q}(r_q,z)=g_{P,0}^{I,q}(r_q,z)=0$$
$$\delta_D=\delta_1=\delta_3=d,\quad \delta_5=d^2,\quad \delta_P=1 \tag{2.16}$$

The potential function in (2.15) has been formulated in such a way that at the vertical exterior boundary of the body q,$r_q=a_q$, the function $\Psi_{D,m}^{I,q}$ can be reduced to simple Fourier series. This facilitates the formulation and the numerical implementation of the matching condition for the diffraction velocity potential in $r_q=a_q$. For this reason the second term in the expression $g_{D,m}^{I,q}(r_q,z)$ has been introduced as in Garret (1971), Kokkinowrachos et al. (1986), Mavrakos (1985).

In (2.15) and (2.16), H_m and K_m is the m-th order Hankel function of the first kind and the modified Bessel function of the second type, respectively, whereas $Z_n(z)$ are orthonormal functions in [0, d] defined by (2.11) for n=0 and:

$$Z_n(z)=\left[\frac{1}{2}\cdot\left[1+\frac{\sin(2a_nd)}{2a_nd}\right]\right]^{-1/2}\cdot\cos(a_nz),\quad n\neq 0 \tag{2.17}$$

a_n being the roots of the transcendental equation

$$\frac{\omega^2}{g}+a_n\tan(a_nd)=0 \tag{2.18}$$

which possesses one imaginary, $a_n=-ik$, $k>0$, and infinite number of real roots. Substituting the value of a_0 in Eqs. (2.17) and (2.18), Eq. (2.11) and the dispersion equation can directly be obtained. Moreover, since for $a_0=-ik$ (Abramowitz and Stegun,

1970):

$$K_m(-ikr_p)=\frac{\pi}{2}i^{m+1}H_m(kr_p) \tag{2.19}$$

the first term in the series expansion in (2.15) behaves as outgoing wave at large r satisfying the radiation condition. For $n\geq 1$, the remaining terms in (2.15) represent evanescent waves exponentially decaying at large r.

At this point, it should be mentioned that the motion-and pressure-radiation potentials ϕ_j^q and ϕ_P^q, see Eqs. (2.13) and (2.14) respectively, around the isolated body q involve a single value of m depending on the mode of motion and the problem considered. So, $m=0$ stands for the symmetric modes of motion, i.e. for the heave- and pressure-radiation problems (Mavrakos, 1991; Mavrakos and Konispoliatis, 2012), while $m=\pm 1$ refers to the antisymmetric motion-radiation problems (surge, sway, roll and pitch). However, the series representations in the form of Eqs. (2.13) and (2.14) have been preferred at this stage of the analysis in order to attain similar representations with the ones of the total potentials, ϕ_j^{qp} and ϕ_P^{qp}, induced around any body q of the multi-body configuration due to the oscillation of body p in the j-th direction in otherwise calm water (motion-dependent radiation potential) or due to the time harmonic oscillating pressure head inside the air chamber of body p (pressure-dependent radiation potential) respectively. These potentials, expressed in the q–th body's cylindrical coordinate system (r_q,θ_q,z), include components for all values of m accounting for interference effects.

2.2. Multiple scattering approach for the velocity potential representation of interacting OWC's devices

In accordance to Eqs. (2.13) and (2.14) the afore mentioned potentials, ϕ_j^{qp},($j=1,\ldots,6,P$) in a multi-body configuration can be expressed in the q–th body's cylindrical coordinate system, as:

$$\phi_j^{qp}(r_q,\theta_q,z)=-i\omega\sum_{m=-\infty}^{\infty}\Psi_{j,m}^{qp}(r_q,z)\cdot e^{im\theta_q} \tag{2.20}$$

$$\phi_P^{qp}(r_q,\theta_q,z)=\frac{1}{i\omega\rho}\sum_{m=-\infty}^{\infty}\Psi_{P,m}^{qp}(r_q,z)\cdot e^{im\theta_q} \tag{2.21}$$

Here, the functions $\Psi_{j,m}^{qp}(r_q,z)$, ($j=1,2,\ldots,6,P$) are the principal unknown of the problem. In order to express the potentials, ϕ_j^{qp}, in the form of Eqs. (2.20) and (2.21), use is made of the multiple scattering approach (Twersky, 1952; Okhusu, 1974). The method accounts for the hydrodynamic interaction phenomena among the devices in the array by superposing to the isolated body potential flow solution various orders of scattered/radiated wave fields emanating from the rest of the devices. The implementation of the multiple scattering formulation for the solution of the diffraction and the motion-dependent radiation problems around arbitrarily shaped, floating or/and submerged vertical axisymmetric bodies has been extensively reported in the literature (see Mavrakos and Koumoutsakos, 1987; Mavrakos, 1991) and thus, it will be no further elaborated here.

In this section, the implementation of the physical idea of multiple scattering for solving the pressure-depended radiation problem for an array of hydrodynamically interacting OWC's devices will be presented. In doing this, we initially consider the device p ($p=1,2,\ldots,N$) of the arrangement subjected to time harmonic oscillating air chamber pressure head with unit amplitude, the rest of the devices, $q=1,2,\ldots,N;\ q\neq p$, being considered restrained in the wave field and open to the atmosphere. Due to the existence of the inner pressure, the body p radiates its "zero order of radiation", ${}^0\phi_P^{pp}$, given by Equations (2.14)–(2.16), such that the latter is the solution of the non-homogeneous pressure-dependent radiation problem expressed in the cylindrical coordinate system of body p, see Eq. (2.5). Thus:

$$\sum_{p=1}^{N}{}^0\phi_P^{pp}$$

is the total velocity potential radiated by the entire multi-device configuration in the absence of interaction phenomena. The radiation potential ${}^0\phi_P^{pp}$, represents a "first order of incident wave", ${}^1\phi_{0,P}^{qp}$, for each of the remaining devices of the arrangement, ($q=1,2,\ldots,N;\ q\neq p$), which have been considered restrained in the waves and open to the atmosphere, in response to which they radiate a "first order of scattering", ${}^1\phi_{7,P}^{qp}$,($q=1,2,\ldots,N;\ q\neq p$). Here the subscript 0, denotes incident wave on the device q, emanating from body p due to its own unit pressure head (i.e. superscript pp), while the subscript P, denotes the pressure radiation problem. The subscript 7 denotes the scattered waves from device q in accordance to the notation used in Eq. (2.2). The corresponding total "first order potential" around the device q due to the unit inner air pressure head in device p, is equal to:

$${}^1\phi_P^{qp}={}^1\phi_{7,P}^{qp}+{}^1\phi_{0,P}^{qp},\quad q\neq p$$

The above "first order potential" has to satisfy homogeneous boundary conditions on the restrained device q (Eq. (2.7)), with atmospheric inner pressure, i.e.:

$$\omega^2\cdot{}^1\phi_P^{qp}-g\partial^1\frac{\phi_P^{qp}}{\partial z}=\left\{\begin{array}{lll}0 & \text{for} & r_q\geq a_q\\ 0 & \text{for} & 0\leq r_q\leq b_q\end{array}\right\} \tag{2.22}$$

Especially for the device p, with unit inner air pressure head, the "first order" of incident and scattered wave potentials, denoted by ${}^1\phi_{0,P}^{pp}$, ${}^1\phi_{7,P}^{pp}$ respectively, do not exist in the context of the present formulation. Indeed, since the remaining devices of the arrangement are considered restrained (Eq. (2.7)) in the wave field and open to the atmosphere when body p is subjected to inner pressure head, they do not radiate any potential of "zero order" at all, which would contribute to the "first order of incident wave", on the p device, i.e. ${}^0\phi_P^{pq}={}^1\phi_{0,P}^{pq}=0$ for $q=1,2,\ldots,N,\ q\neq p$.

Next, in response to all the waves of the "first order of scattering" from the remaining devices, which can be considered as a "second order of incident wave" ${}^2\phi_{0,P}^{qp}$, for the device q ($q=1,2,\ldots,N$), i.e.

$${}^2\phi_{0,P}^{qp}=\sum_{l=1}^{N}(1-\delta_{l,q})\cdot{}^1\varphi_{7,P}^{lp} \tag{2.23}$$

the q device radiates a wave of "second order of scattering", denoted by ${}^2\phi_{7,P}^{qp}$, such that the total "second order potential", ${}^2\phi_P^{qp}={}^2\phi_{7,P}^{qp}+{}^2\phi_{0,P}^{qp}$, satisfies the homogeneous boundary conditions on the restrained body in the q-th coordinate system and with atmospheric pressure head in its air chamber (see Eqs. (2.22) and (2.7)). The same homogeneous conditions remain valid for all the higher order interaction potentials ${}^s\phi_P^{qp}$, $s\geq 1$, even in the case when the device q coincides with the device p having unit inner pressure head in its air chamber. Indeed, as the non-homogeneous free surface condition in the device $p\equiv q$ has been already fulfilled through the solution of zero order, ${}^0\phi_P^{pp}$, i.e. $\omega^2\cdot{}^0\phi_P^{pp}-g\partial^0\frac{\varphi_P^{pp}}{\partial z}=\left\{\begin{array}{lll}0 & \text{for} & r_q\geq a_q\\ -\frac{i\omega}{\rho} & \text{for} & 0\leq r_q\leq b_q\end{array}\right\}$(see also Eq. (2.5)), it is sufficient to require that for all the potentials of higher order of interaction ${}^s\phi_P^{pp}$, $s\geq 1$, it holds:

$$\omega^2\cdot{}^s\phi_P^{pp}-g\partial^s\frac{\phi_P^{pp}}{\partial z}=\left\{\begin{array}{lll}0 & \text{for} & r_q\geq a_q\\ 0 & \text{for} & 0\leq r_q\leq b_q\end{array}\right\} \tag{2.24}$$

Following the same procedure, we produce the sth order of interaction for any device q ($q=1,2,\ldots,N$) of the arrangement. Thus, the corresponding sth order incident, ${}^s\phi_{0,P}^{qp}$, scattered, ${}^s\phi_{7,P}^{qp}$ and

total wave potential, will be:

$$ {}^{s}\phi_{0,P}^{qp} = \sum_{l=1}^{N} (1-\delta_{l,q}) \cdot {}^{s-1}\phi_{7,P}^{lp}, \text{for} \geq 1; {}^{s}\phi_{P}^{qp} = {}^{s}\phi_{7,P}^{qp} + {}^{s}\phi_{0,P}^{qp} \quad (2.25) $$

where ${}^{s}\phi_{P}^{qp}$, for $s \geq 1$, satisfies the boundary condition on the restrained device with atmospheric inner pressure, as mentioned previously (see Eqs. (2.22) and (2.7)). Assuming that s is approaching to infinity and summing over the various interaction orders, the total radiated wave scattered from and incident to the q device, denoted by $\phi_{7,P}^{qp}, \phi_{0,P}^{qp}$, respectively, are:

$$ \phi_{7,P}^{qp}(r_q,\theta_q,z) = \delta_{q,p}\,{}^{0}\phi_{P}^{pp}(r_p,\theta_p,z) + \sum_{s=1}^{\infty} {}^{s}\phi_{7,P}^{qp}(r_q,\theta_q,z) \quad (2.26) $$

$$ \phi_{0,P}^{qp}(r_q,\theta_q,z) = \sum_{s=1}^{\infty} {}^{s}\phi_{0,P}^{qp}(r_q,\theta_q,z) = \sum_{s=1}^{\infty}\sum_{l=1}^{N}(1-\delta_{l,q}) \cdot {}^{s-1}\phi_{7,P}^{lp} \quad (2.27) $$

The total wave field ϕ_{P}^{qp}, induced around any device q of the multi–component configuration due to the unit inner air pressure in device p, can be written as:

$$ \phi_{P}^{qp} = \phi_{0,P}^{qp} + \phi_{7,P}^{qp} = \delta_{q,p}\,{}^{0}\phi_{P}^{pp} + \sum_{s=1}^{\infty}\left[{}^{s}\phi_{7,P}^{qp} + {}^{s}\phi_{0,P}^{qp}\right] = \delta_{q,p}\,{}^{0}\phi_{P}^{pp} + \sum_{s=1}^{\infty}\left[{}^{s}\phi_{7,P}^{qp} + \sum_{l=1}^{N}(1-\delta_{lq}) \cdot {}^{s-1}\phi_{7,P}^{lp}\right] = \delta_{q,p}\,{}^{0}\phi_{P}^{pp} + \sum_{s=1}^{\infty} {}^{s}\phi_{P}^{qp} \quad (2.28) $$

The velocity potential ϕ_{P}^{qp} will satisfy the imposed boundary conditions in the coordinate frame of the q device ($q=1,2,\ldots,N$). Indeed, in cases where the device q coincides with the device p with unit inner air pressure, the appropriate non-homogeneous free surface boundary condition inside the device p, see Eq. (2.5), is satisfied by the first term on the rhs of Eq. (2.28) ${}^{0}\phi_{P}^{pp}$. Each of the remaining terms, ${}^{s}\phi_{P}^{qp}$, involved in the infinite series in (2.28), are selected so that they fulfill homogeneous free surface boundary conditions inside and outside any device of the configuration (see Eqs. (2.22) and (2.24)), the latter being considered restrained in the waves and open to the atmosphere, and thus the terms ${}^{s}\phi_{P}^{qp}$ do not affect the validity of the imposed boundary condition for the device p with unit inner pressure. On the other hand, if the device q is open to the atmosphere, the homogeneous free-surface boundary condition (Eq. (2.5)) will also be satisfied by ϕ_{P}^{qp} since-according to the preceding analysis–all ${}^{s}\phi_{P}^{qp}$,$(s=1,2,\ldots)$ satisfy the same homogeneous condition, see Eqs. (2.22) and (2.24), as well and ${}^{0}\phi_{P}^{pp}$ will be absent in this case. In this way, the problem is reduced to the determination of the unknown potentials ${}^{s}\phi_{P}^{qp}$, which through Eq. (2.25) are expressed as a superposition of the sth order wave scattered by the device q, ${}^{s}\phi_{7,P}^{qp}$, and the $(s-1)$th order waves scattered by the remaining devices ${}^{s-1}\phi_{7,P}^{lp}, l = 1,2,\ldots,N; l \neq q$.

Each order of scattered wave potential ${}^{s}\phi_{7,P}^{qp}$, $s \geq 1$, contributing to ${}^{s}\phi_{P}^{qp}$,$(q=1,2,\ldots,N)$ can be described in terms of cylindrical wave functions as (Konispoliatis and Mavrakos, 2013):

$$ {}^{s}\phi_{7,P}^{qp}(r_q,\theta_q,z) = \frac{1}{i\omega\rho}\sum_{m=-\infty}^{\infty} {}^{s}\Psi_{7,P,m}^{qp}(r_q,z) \cdot e^{im\theta_q} \quad (2.29) $$

where for the outer fluid domain of the device q, i.e. $r_q \geq a_q, 0 \leq z \leq d$:

$$ {}^{s}\Psi_{7,P,m}^{qp}(r_q,z) = \sum_{j=0}^{\infty} {}^{s}F_{P,m,j}^{I,qp}\frac{K_m(a_j r_q)}{K_m(a_j a_q)} \cdot Z_j(z) \quad (2.30) $$

All functions and symbols appearing in (2.30) have been introduced previously in Eqs. (2.15)–(2.19). The sth order scattering coefficients ${}^{s}F_{P,m,j}^{I,qp}$, are obtained through the solution of the respective order of the diffraction problem around the device q with inner atmospheric pressure in the qth coordinate system. Thus the potential ${}^{s}\phi_{P}^{qp}$, around the device q can be found by substitution of Eq. (2.29) in Eq. (2.25).

At this point, it should be mentioned that each of the scattered waves ${}^{s-1}\phi_{7,P}^{lp}, l = 1,2,\ldots,N$, contributing to ${}^{s}\phi_{P}^{qp}$, are expressed in terms of different coordinates. Using a Bessel function addition theorem, all velocity potentials expressed in the (r_l,θ_l,z) coordinates may be transformed to expressions in the reference coordinates of the device q (Watson, 1966):

$$ K_\nu(a_j r_\ell) \cdot e^{i\nu\theta_\ell} = \sum_{m=-\infty}^{\infty} (-1)^m \cdot K_{\nu-m}(a_j \ell_{\ell q}) \cdot I_m(a_j r_q) \cdot e^{i(\nu-m)\theta_{\ell q}} \cdot e^{im\theta_q}, for\ r_\ell < \ell_{\ell q} \quad (2.31) $$

here I_m denotes the mth order modified Bessel function of first kind.

Using the relations $I_m(-ikr_q) = (-i)^m \cdot J_m(kr_q)$, $K_m(-ikr_q) = \pi/2\, i^{m+1} \cdot H_m(kr_q)$ (Abramowitz and Stegun, 1970), for the imaginary root $a_j = -ik$, the Eq. (2.31) can be written as:

$$ H_\nu(kr_\ell) \cdot e^{i\nu\theta_\ell} = \sum_{m=-\infty}^{\infty} H_{\nu-m}(k\ell_{\ell q}) \cdot J_m(kr_q) \cdot e^{i(\nu-m)\theta_{\ell q}} \cdot e^{im\theta_q} \quad (2.32) $$

Using the expressions (2.31), (2.32), all the terms of the sth order total wave field, given by Eq. (2.25), can be expressed in the coordinate frame of the q device, in all the fluid domains ($k=I,III$ and M, see Fig. 1), i.e.

$$ {}^{s}\phi_{P}^{qp}(r_q,\theta_q,z) = \frac{1}{i\omega\rho}\sum_{m=-\infty}^{\infty} {}^{s}\Psi_{P,m}^{k,qp}(r_q,z) \cdot e^{im\theta_q}, \quad k = I, III, M \quad (2.33) $$

Here the function ${}^{s}\Psi_{P,m}^{k,qp}$ for the outer fluid domain is given by:

$$ {}^{s}\Psi_{P,m}^{I,qp}(r_q,z) = \sum_{j=0}^{\infty}\left[{}^{s}G_{P,m,j}^{I,qp}\frac{I_m(a_j r_q)}{I_m(a_j a_q)} + {}^{s}F_{P,m,j}^{I,qp}\frac{K_m(a_j r_q)}{K_m(a_j a_q)}\right] \cdot Z_j(z) \quad (2.34) $$

where

$$ {}^{s}G_{P,m,j}^{I,qp} = \sum_{i=1}^{N}(1-\delta_{\ell,q})\sum_{\nu=-\infty}^{\infty} i^{m+\nu}\frac{K_{\nu-m}(a_j \ell_{qp}) I_m(a_j a_q)}{K_\nu(a_j a_q)}\left({}^{s-1}F_{P,\nu,j}^{I,\ell p}\right) \cdot e^{i(\nu-m)\theta_{\ell q}} \quad (2.35) $$

Next, with the help of Eqs. (2.34) and (2.35), the total wave field, given by Eq. (2.28), can be expressed in the form of Eq. (2.21) where:

$$ \Psi_{P,m}^{I,qp}(r_q,z) = \delta_{q,p}\Psi_{P,m}^{I,p}(r_p,z) + \sum_{j=0}^{\infty}\left[G_{P,m,j}^{I,qp}\frac{I_m(a_j r_q)}{I_m(a_j a_q)} + F_{P,m,j}^{I,qp}\frac{K_m(a_j r_q)}{K_m(a_j a_q)}\right] \cdot Z_j(z) \quad (2.36) $$

$$ G_{P,m,j}^{I,qp} = \sum_{s=1}^{\infty} {}^{s}G_{P,m,j}^{I,qp}, F_{P,m,j}^{I,qp} = \sum_{s=1}^{\infty} {}^{s}F_{P,m,j}^{I,qp}, \text{ and } \Psi_{P,m}^{I,p}(r_p,z) = \sum_{j=0}^{\infty} F_{P,m,j}^{I}\frac{K_m(a_j r_p)}{K_m(a_j a_p)} \cdot Z_j(z) \quad (2.37) $$

The corresponding expressions for the total velocity potential in the III and M fluid domain are given in the Appendix A.

3. Determination of the Fourier coefficients for the pressure-radiation problem

The condition for continuity of the potential function $\phi_{P}^{\ell}(\ell = qp; p, q = 1,\ldots,N)$ at $r_q = b_q; r_q = a_q$, and its radial derivative are expressed by:

$$ \Psi_{P,m}^{III,\ell}(b_q,z) = \Psi_{P,m}^{M,\ell}(b_q,z) \quad (3.1) $$

$$ \left.\frac{\partial\Psi_{P,m}^{III,\ell}}{\partial r}\right|_{r=b_q} = \left.\frac{\partial\Psi_{P,m}^{M,\ell}}{\partial r}\right|_{r=b_q} \quad (3.2) $$

$$ \Psi_{P,m}^{I,\ell}(a_q,z) = \Psi_{P,m}^{III,\ell}(a_q,z) \quad (3.3) $$

$$\left.\frac{\partial \Psi_{P,m}^{I,\ell}}{\partial r}\right|_{r=a_q} = \left.\frac{\partial \Psi_{P,m}^{III,\ell}}{\partial r}\right|_{r=a_q} \tag{3.4}$$

Multiplying both sides of Eqs. (3.1) and (3.3) by $(1/h_q)\cos(s\pi z/h_q)$ and integrating over their region of validity,$[0,h_q]$, the following set of equations can be obtained:

$$F_{P,m,n}^{*III,qp} = \delta_{q,p} Q_{P,0,n}^{*} + \sum_{i=0}^{\infty} L_{n,i} F_{P,m,i}^{M,qp} \ for \ 0 \le z \le h_q, r = b_q \tag{3.5}$$

$$F_{P,m,n}^{III,qp} = \sum_{i=0}^{\infty} F_{P,m,i}^{I,qp} L_{n,i} \ for \ 0 \le z \le h_q, r = a_q \tag{3.6}$$

where $L_{n,i}$ and $Q_{p,0,n}^{*}$ are defined in Appendix B.

The condition for the continuity of the radial derivative of the potential at $r_q = b_q; r_q = a_q$, as expressed by Eqs. (3.2), (3.4), respectively, as well as the kinematic condition on the vertical boundaries of the q device, as described by Eq. (2.8) must be fulfilled too. Multiplying both sides of Eqs. (3.2), (3.4), (2.8) with the weight function $(1/d)Z_\mu(z)$, integrating over the region of their validity, that is $[0,h_q]$ and $[h_q,d]$, respectively, and adding the resulting expressions, the following set of equations is obtained:

$$\sum_{i=0}^{\infty} F_{P,m,i}^{M,qp} A_{m,i}^{M} = \frac{h_q}{d} \sum_{n=0}^{\infty} \varepsilon_n L_{n,i} \left(D_{m,n}^{III,qp} F_{P,m,n}^{III,qp} + D_{m,n}^{*III,qp} F_{P,m,n}^{*III,qp} \right), for \ r = b_q \tag{3.7}$$

$$\sum_{i=0}^{\infty} \left(F_{P,m,i}^{I,qp} A_{m,i}^{I} + D_{m,i}^{I} \right) \delta_{i,\mu} = \frac{h_q}{d} \sum_{n=0}^{\infty} \varepsilon_n L_{n,i} \left(A_{m,n}^{III,qp} F_{P,m,n}^{III,qp} + A_{m,n}^{*\ III,qp} F_{P,m,n}^{*III,qp} \right), for \ r = a_q \tag{3.8}$$

where $A_{m,i}^{M}, D_{m,n}^{III,qp}, D_{m,n}^{*III,qp}, A_{m,i}^{I}, A_{m,n}^{III,qp}, A_{m,n}^{*III,qp}$ and $D_{m,i}^{I}$ are defined in Appendix B and ε_n is the Neumann's symbol defined as $\varepsilon_0 = 1$, for $n=0$; otherwise $\varepsilon_n = 2$.

For the numerical implementation of the method, series (2.36), (A1) and (A3) expressing the potential around the q device in I, III, M fluid region will be truncated after Q, M, N terms, respectively.

The substitution of Eq. (3.5) into Eq. (3.7) will provide the unknown Fourier coefficients in the M fluid domain in relation with the Fourier coefficients in the III fluid domain, in the following matrix form, that is:

$$\left\{F_{P,m,i}^{M,qp}\right\} = \frac{h_q}{d}\left[G_{i,i}^{qp}\right]^{-1} \cdot \left[L_{i,n}^{M,III}\right] \cdot [\varepsilon_n] \cdot \left[D_{m,n}^{III,qp}\right] \cdot \left\{F_{P,m,n}^{III,qp}\right\} + \frac{h_q}{d}\left[G_{i,i}^{qp}\right]^{-1} \cdot \left[L_{i,n}^{M,III}\right] \cdot [\varepsilon_n] \cdot \left[D_{m,n}^{*\ III,qp}\right] \cdot \left\{Q_{P,0,n}^{*}\right\} \tag{3.9}$$

where $\left[G_{i,i}^{qp}\right]$, is a $N \times N$ square matrix equal to:

$$\left[G_{i,i}^{qp}\right] = \left[A_{m,i}^{M}\right] - \frac{h_q}{d}\left[L_{i,n}^{M,III}\right] \cdot [\varepsilon_n] \cdot \left[D_{m,n}^{*\ III,qp}\right] \cdot \left[L_{n,i}^{III,M}\right] \tag{3.10}$$

Here, $\left\{F_{P,m,i}^{M,qp}\right\}, \left\{F_{P,m,n}^{III,qp}\right\}$ are both complex vectors, the elements of which are the unknown Fourier coefficients in the M and III fluid domain, respectively around the q device, $\left[A_{m,i}^{M}\right]$ is a $(N \times N)$ diagonal matrix given by (B5), $\left[L_{i,n}^{M,III}\right]$ is a $(N \times M)$ matrix given by (B1)–(B3), $[\varepsilon_n]$ is a $(M \times M)$ diagonal matrix containing the Neumann's symbol, $\left[D_{m,n}^{III,qp}\right]$ and $\left[D_{m,n}^{*III,qp}\right]$ are $(M \times M)$ diagonal matrices defined by Eq. (B7) in the Appendix B and $\left\{Q_{P,0,n}^{*}\right\}$ is a column vector $(M \times 1)$ defined by Eq. (B4) in Appendix B too.

Substituting Eq. (3.9) into Eq. (3.5) the Fourier coefficients in the III fluid domain are connected with the bellow relation:

$$\left\{F_{P,m,n}^{*III,qp}\right\} = \frac{h_q}{d}\left[L_{n,i}^{III,M}\right] \cdot \left[G_{i,i}^{qp}\right]^{-1} \cdot \left[L_{i,n}^{M,III}\right] \cdot [\varepsilon_n] \cdot \left[D_{m,n}^{III,qp}\right] \cdot \left\{F_{P,m,n}^{III,qp}\right\} + \left([I] + \frac{h_q}{d}\left[L_{n,i}^{III,M}\right] \cdot \left[G_{i,i}^{qp}\right]^{-1} \cdot \left[L_{i,n}^{M,III}\right] \cdot [\varepsilon_n] \cdot \left[D_{m,n}^{*\ III,qp}\right]\right)\left\{Q_{P,0,n}^{*}\right\} \tag{3.11}$$

where $[I]$ is the unit matrix.

Finally, the substitution of the Eq. (3.6) into Eq. (3.8) will provide the unknown Fourier coefficients in the I fluid domain, in the following matrix form:

$$[E_{i,i}] \cdot \left\{F_{P,m,i}^{I,qp}\right\} = \{B\} \tag{3.12}$$

where

$$\{B\} = \left[D_{m,i}^{I}\right] - \frac{h_q}{d}\left[L_{i,n}^{I,III}\right] \cdot [\varepsilon_n] \cdot \left(\left[A_{m,n}^{*III,qp}\right] + \frac{h_q}{d}\left[A_{m,n}^{*III,qp}\right] \cdot \left[L_{n,i}^{III,M}\right] \cdot \left[G_{i,i}\right]^{-1} \cdot \left[L_{i,n}^{M,III}\right] \cdot [\varepsilon_n] \cdot \left[D_{m,n}^{*III,qp}\right] \right) \cdot \left\{Q_{P,0,n}^{*}\right\} \tag{3.13}$$

$$[E_{i,i}] = \frac{h_q}{d}\left(\left[L_{i,n}^{I,III}\right] \cdot [\varepsilon_n] \cdot \left(\left[A_{m,n}^{III,qp}\right] + \frac{h_q}{d}\left[A_{m,n}^{*III,qp}\right] \cdot \left[L_{n,i}^{III,M}\right] \cdot \left[G_{i,i}\right]^{-1} \cdot \left[L_{i,n}^{M,III}\right] \cdot [\varepsilon_n] \cdot \left[D_{m,n}^{III,qp}\right] \right) \right) \cdot \left[L_{n,i}^{III,I}\right] - \left[A_{m,i}^{I}\right] \tag{3.14}$$

Here $\left[A_{m,n}^{III,qp}\right]$ and $\left[A_{m,n}^{*III,qp}\right]$ are $(M \times M)$ diagonal matrices defined by Eq. (B8), $\left[A_{m,i}^{I}\right]$ and $\left[D_{m,i}^{I}\right]$ are $(Q \times Q)$ diagonal matrices given by (B6) and (B9), respectively in Appendix B.

Having the system of Eqs. (3.9), (3.11) and (3.12) solved the Fourier coefficients for the pressure-dependent radiation problem for the device q of the array, in all fluid domains can be determined.

4. Volume flow

The water oscillation inside each device's chamber pushes the dry air above the free surface through a Wells turbine. The volume flow produced by the oscillating internal water surface in the q device $(q=1,2,\ldots,N)$ is denoted by $Q^q(t) = \mathrm{Re}\{q^q \cdot e^{-i\omega t}\}$ where:

$$q^q = \iint_{S_i^q} u_z^q dS_i^q = \iint_{S_i^q} u_z^q(r_q,\theta_q,z) r_q dr_q d\theta_q = \iint_{S_i^q} \frac{\partial \phi^q}{\partial z} r_q dr_q d\theta_q \tag{4.1}$$

here u_z^q denotes the vertical velocity of the water free surface in the q device and S_i^q the cross-sectional area of the inner water surface inside the q device.

Since the spatial function ϕ^q was decomposed into three terms, see Eq. (2.2), it proves convenient to follow the same procedure and decompose the volume flow q^q, in the q device into three terms associated with the diffraction q_D^q, the motion-dependent,q_R^q, and the pressure-dependent, q_P^q, radiation problem, as follows (Falnes and McIver, 1985):

$$q^q = q_D^q + q_R^q + \sum_{p=1}^{N} p_{in0}^{p} \cdot q_p^{qp} \tag{4.2}$$

We shall call the complex quantity q_p^{qp} the radiation admittance, as introduced first by Evans (1982) where:

$$q_p^{qp} = -g_p^{qp} + i f_p^{qp} \tag{4.3}$$

Here g_p^{qp}, f_p^{qp} are respectively, the radiation conductance and the radiation susceptance. Assuming uniform pressure distribution inside the chamber, same as for an isolated device (Mavrakos and Konispoliatis, 2012), only the pumping mode for $m=0$ affects the volumetric oscillations in evaluating the q_p^{qp}. Moreover, by substituting the diffraction potential around the q device after using the multiple scattering approach (Mavrakos, 1996) into Eq. (4.1) it can be shown that only modes with $m=0$ contribute to q_D^q. Finally, the volume flow rate due to the motion-dependent radiation problem can be expressed on the basis of the relative vertical displacement between the internal free surface elevation and the

motions of the q device, i.e. (Falnes and McIver, 1985)

$$q_R^q = \sum_{p=1}^{N}\sum_{j=1}^{6} \dot{\xi}_{j0}^p q_{3,j}^{qp} - \dot{\xi}_{30}^q S_i^q \tag{4.4}$$

here $q_{3,j}^{qp}$ denotes the volume flow into the chamber of the q device due to the motion-dependent radiation problem, originating from the motion of the p device in the j direction. These complex coefficients represent the hydrodynamic coupling between the oscillating OWC devices and the oscillating pressure distributions (Falnes and McIver, 1985). As in an isolated device (Mavrakos and Konispoliatis, 2012) only the vertical displacement of the q device of the array contribute to its volume flow. In addition, the motions in 6 degrees of freedom of the p device of the array affect the volume of air in q devices' chamber. Thus all 6 motions/rotations of the N devices contribute to the volume flow rate of q device.

The Eq. (4.2) for all the N devices of the arrangement can be written in the following matrix form, that is:

$$[q^N] = [q_D^N] + \left[q_j^N\right] \cdot \left[\dot{\xi}_{j0}^N\right] + \left[q_p^N\right] \cdot [p_{in0}^N] \tag{4.5}$$

where $[q^N], [q_D^N]$ are column matrices $(N \times 1)$ containing the total volume flows and the volume flows associated with the diffraction problem, respectively, in all the devices; $\left[q_j^N\right]$ is a $(N \times 6N)$ matrix containing the volume flows in all the devices due to the forced oscillation of each device with unit velocity amplitude (motion-dependent radiation problem); $\left[q_P^N\right]$ is a $(N \times N)$ square matrix containing the volume flows in all the devices due to pressure-dependent radiation problem; $\left[\dot{\xi}_{j0}^N\right]$ is a column matrix $(6N \times 1)$ containing the velocities in the 6 degrees of freedom of all the devices of the configuration; and $[p_{in0}^N]$ is a column matrix $(N \times 1)$ containing the values of the inner air pressure in each device of the array.

A Wells turbine is assumed to be placed in each devices' duct between the chamber and the outer atmosphere since it rotates in one direction in spite the direction of the air flow. For simplicity, we represent the turbine in the device q by a pneumatic complex admittance Λ^q. The total volume flow,q^q, in the q device is proportional to the chamber air pressure (Evans and Porter, 1996; Falnes, 2002):

$$q^q = \Lambda^q \cdot p_{in0}^q \tag{4.6}$$

Assuming isentropy so that variations of air density and pressure are proportional to each other with $c_{air}^2 = dp_{in}^q/d\rho_{air}$, c_{air} being the sound velocity in air, the pneumatic complex admittance Λ^q is equal to (Sarmento and Falcao, 1985):

$$\Lambda^q = \frac{KD}{N\rho_{air}^0} - i\omega\frac{V_0^q}{c_{air}^2\rho_{air}^0} \tag{4.7}$$

here N is the rotational speed of turbine blades, D the outer diameter of turbine rotor, ρ_{air}^0 the static air density and V_0^q the q device's air chamber volume. The empirical coefficient K depends on the design, the setup and the number of turbines.

The real part of Λ^q is related to the pressure drop through the turbine; whereas the imaginary part of Λ^q represents the effect of the air compressibility inside the chamber of each OWC device, thus it is negligible as long as the effect of air compressibility is disregarded. As shown by Sarmento and Falcao (1985) and subsequently by Martins–Rivas and Mei (2009a, 2009b) and Gomes et al. (2012) air compressibility can have a non-negligible effect on the power extraction of an OWC device and create a time lag between the variation of the volume flow and the variation of the inner air pressure thus it should not be neglected in full scale OWC projects. For the sake of validation of our numerical results (see Section 10) with those of other researchers, the air compressibility is neglected in the present study, and thus, the pneumatic admittance Λ^q is considered to be real number.

5. Wave forces

The various forces on each device q of an array of N OWC devices can be calculated from the pressure distribution given by the linearized Bernoulli's equation:

$$P(r_q, \theta_q, z; t) = -\rho\frac{\partial \Phi^q}{\partial t} = -i\omega\rho\phi^q \cdot e^{-i\omega t} \tag{5.1}$$

where ϕ^q is the velocity potential of the device q in each fluid domain.

The first order horizontal exciting forces acting on the q device can be calculated by integrating the hydrodynamic pressure on the external and the internal device's vertical walls, i.e.

$$f_x^q = f_{x_{Out}}^q - f_{x_{In}}^q = -i\omega\rho a_q \int_{z=h_q}^{z=d}\int_0^{\theta=2\pi} \phi^{I,q} \cos\,\theta_q d\theta_q dz + i\omega\rho b_q \int_{z=h_q}^{z=d}\int_0^{\theta=2\pi} \phi^{M,q} \cos\,\theta_q d\theta_q dz \tag{5.2}$$

$$f_y^q = f_{y_{Out}}^q - f_{y_{In}}^q = -i\omega\rho a_q \int_{z=h_q}^{z=d}\int_0^{\theta=2\pi} \phi^{I,q} \sin\,\theta_q d\theta_q dz + i\omega\rho b_q \int_{z=h_q}^{z=d}\int_0^{\theta=2\pi} \phi^{M,q} \sin\,\theta_q d\theta_q dz \tag{5.3}$$

The first order vertical exciting force acting on the q device's horizontal walls equals to:

$$f_z^q = -i\omega\rho \int_{r=b_q}^{r=a_q}\int_0^{\theta=2\pi} \varphi^{III,q}(-1) r_q d\theta_q dr_q \tag{5.4}$$

The overturning moment on each device q about a horizontal axis lying at an arbitrary distance $z = e$ from the sea bed is the real part of $M \cdot e^{-i\omega t}$, where M is made up of M_s and M_b arising from the pressure distribution on the q device's vertical walls and on its bottom, respectively, (Mavrakos, 1985):

$$M_{s,x}^q = -i\omega\rho a_q \int_{z=h_q}^{z=d}\int_0^{\theta=2\pi} \phi^{I,q}(z-e)\cos\,\theta_q d\theta_q dz + i\omega\rho b_q \int_{z=h_q}^{z=d}\int_0^{\theta=2\pi} \phi^{M,q}(z-e)\cos\,\theta_q d\theta_q dz \tag{5.5}$$

$$M_{s,y}^q = -i\omega\rho a_q \int_{z=h_q}^{z=d}\int_0^{\theta=2\pi} \phi^{I,q}(z-e)\sin\,\theta_q d\theta_q dz + i\omega\rho b_q \int_{z=h_q}^{z=d}\int_0^{\theta=2\pi} \phi^{M,q}(z-e)\sin\,\theta_q d\theta_q dz \tag{5.6}$$

$$M_b^q = -i\omega\rho \int_{r=b_q}^{r=a_q}\int_0^{\theta=2\pi} \phi^{III,q}(-1) r_q^2 d\theta_q dr_q \tag{5.7}$$

6. Motion-and pressure-dependent hydrodynamic reaction forces

The motion-dependent hydrodynamic reaction forces and moments f_{ij}^{qp} acting on the device q in the ith direction due to the forced oscillation of the device p in the jth direction can be obtained by the linearized Bernoulli's equation as:

$$f_{ij}^{qp} = -\dot{\xi}_{j0}^p i\omega\rho \iint_{S_0} \phi_j^{n,qp} n_i^q dS, n = I, III, M \tag{6.1}$$

The generalized normal components n_i^q have been defined through Eq. (2.8) and $\phi_j^{n,qp}$ are calculated depending on which part of the device's wetted surface the integration is being carried out.

The complex force f_{ij}^{qp} may be written in the form (Newman, 1977a):

$$f_{ij}^{qp}=(-b_{ij}^{qp}+i\omega a_{ij}^{qp})\dot{\xi}_{j0}^{p}=(\omega^2 a_{ij}^{qp}+i\omega b_{ij}^{qp})\xi_{j0}^{p}=\omega^2(a_{ij}^{qp}+i/\omega b_{ij}^{qp})\xi_{j0}^{p}$$
$$=\omega^2\pi_{ij}^{qp}\xi_{j0}^{p} \tag{6.2}$$

where a_{ij}^{qp}, b_{ij}^{qp}, are the well-known added mass and damping coefficients, respectively, both real and dependent on frequency ω.

The above Eq. (6.2) can be written in a matrix form as:

$$\left[f_R^{q,N}\right]=\left[\kappa_{ij}^{qN}\right]\cdot\left[\dot{\xi}_{j0}^{N}\right]=\left[\mu_{ij}^{qN}\right]\cdot\left[\xi_{j0}^{N}\right] \tag{6.3}$$

here $\left[\mu_{ij}^{qN}\right]$ is a square matrix $(6N\times 6N)$, where N defines the number of the OWC devices of the array, containing the added mass and damping coefficients (see Eq. (6.2)); $\left[\xi_{j0}^{N}\right]$ is a column matrix $(6N\times 1)$ containing the motions in the 6th degrees of freedom of all the devices of the configuration.

The corresponding pressure-dependent hydrodynamic reaction forces and moments f_{Pj}^{qp} acting on the device q in the jth direction due to air pressure in the device p can be obtained as in Eq. (6.1) by:

$$f_{Pj}^{qp}=-p_{in0}^{p}i\omega\rho\iint_{S_0}\phi_P^{n,qp}n_i^q dS,\quad n=I,III,M \tag{6.4}$$

where $\phi_P^{n,qp}$ are calculated depending on which fluid domain is being examined.

The force f_{Pj}^{qp} may be written in the form:

$$f_{Pj}^{qp}=(-e_{Pj}^{qp}+id_{Pj}^{qp})p_{in0}^{p} \tag{6.5}$$

where e_{Pj}^{qp}, d_{Pj}^{qp}, are real and dependent on frequency ω, representing the hydrodynamic coupling between the oscillating devices and the oscillating pressure distributions.

In a matrix form, Eq. (6.5) can be written as:

$$\left[f_P^{q,N}\right]=\left[C_P^{N}\right]\cdot\left[p_{in0}^{N}\right] \tag{6.6}$$

here $\left[C_P^{N}\right]$ is a $(6N\times N)$ matrix containing the e_{Pj}^{qp}, d_{Pj}^{qp} from Eq. (6.5) and $\left[p_{in0}^{N}\right]$ is a column matrix $(N\times 1)$ containing the values of the inner air pressure in each device of the array.

7. Motion and air pressure determination

The investigation of the equilibrium of the forces acting on the freely floating array of N OWC devices leads to the following system of differential equations of motion in the frequency domain, $(q=1, 2, \ldots, N)$, i.e.:

$$\sum_{p=1}^{N}\sum_{j=1}^{6}(\delta_{p,q}m_{kj}^{q}+a_{kj}^{qp})\cdot\ddot{\xi}_{j0}^{p}+b_{kj}^{qp}\cdot\dot{\xi}_{j0}^{p}+\delta_{p,q}c_{kj}^{q}\cdot\xi_{j0}^{p}+\sum_{p=1}^{N}(e_{pk}^{qp}-id_{pk}^{qp})\cdot p_{in0}^{p}$$
$$=f_k^q+\delta_{k,3}\cdot f_{MP}^{q}, k=1,2\ldots,6 \tag{7.1}$$

where ξ_j^p is the 6-degree displacement vector of the p device of the array; m_{kj}^{q} is the mass matrix of the q device; a_{kj}^{qp} is the frequency–dependent hydrodynamic mass matrix and b_{kj}^{qp} is the frequency–dependent damping matrix of the device q in the k^{th} direction due to the forced oscillation of the device p in the j^{th} direction (see Eq. (6.2)); c_{kj}^{q} is the stiffness matrix; f_k^q represents the exciting force on the q device in the kth direction (see Eqs. (5.2)–(5.7)); the product $(e_{pk}^{qp}-id_{pk}^{qp})\cdot p_{in0}^{p}$, represents the hydrodynamic reaction forces and moments acting on the device q in the kth direction due to air pressure in the device p (see Eq. (6.5)) and f_{MP}^{q} is the force on the horizontal chamber's wall of the q device due to its inner pressure; it is equal to:

$$f_{MP}^{q}=S_i^q\cdot p_{in0}^{q} \tag{7.2}$$

here S_i^q is the cross-sectional area of the inner water surface inside the q device.

Substituting Eqs. (6.5) and (7.2) into Eq. (7.1) we get:

$$\sum_{p=1}^{N}\left\{\sum_{j=1}^{6}\left\{-\omega^2\cdot\left[\delta_{p,q}m_{kj}^{q}+a_{kj}^{qp}+\frac{i}{\omega}b_{kj}^{qp}\right]+\delta_{p,q}c_{kj}^{q}\right\}\cdot\xi_{j0}^{p}\right.$$
$$\left.+\left\{-\frac{f_{Pk}^{qp}}{p_{in0}^{p}}-\delta_{p,q}\delta_{k,3}S_i^q\right\}\cdot p_{in0}^{p}\right\}=f_k^q, k=1,2\ldots,6 \tag{7.3}$$

In a matrix form Eq. (7.3) can be written as:

$$\left[\mu^{N}\right]\cdot\left[\ddot{\xi}_{j0}^{N}\right]+\left[C^{N}\right]\cdot\left[p_{in0}^{N}\right]=\left[f_D^{N}\right] \tag{7.4}$$

where $\left[C^{N}\right]$ is a $(6N\times N)$ matrix containing the $(-f_{Pk}^{qp}/p_{in0}^{p}-\delta_{p,q}\delta_{k,3}S_c^q)$ elements; $\left[\mu^{N}\right]$ is a square $(6N\times 6N)$ matrix containing the elements $\left(-\omega^2\cdot\left[\delta_{p,q}m_{kj}^{q}+a_{kj}^{qp}+\frac{i}{\omega}b_{kj}^{qp}\right]+\delta_{p,q}c_{kj}^{q}\right)$; $\left[f_D^{N}\right]$ is a $(6N\times 1)$ vector containing the exciting forces acting on each device of the array; the vectors $\left[\ddot{\xi}_{j0}^{N}\right]$, $\left[p_{in0}^{N}\right]$ are defined by Eqs. (6.3) and (6.6).

From Eqs. (4.5) and (4.6) we get:

$$\left[\lambda^{N}\right]\cdot\left[\ddot{\xi}_{j0}^{N}\right]+\left[B^{N}\right]\cdot\left[p_{in0}^{N}\right]=\left[q_D^{N}\right] \tag{7.5}$$

Here $\left[B^{N}\right]$ is a $(N\times N)$ square matrix; it is equal to $\left[B^{N}\right]=\left[\Lambda^{N}\right]-\left[q_p^{N}\right]$, where $\left[\Lambda^{N}\right]$ is a $(N\times N)$ diagonal matrix containing the $(\delta_{p,q}\Lambda^{q})$ elements (see Eqs. (4.5), (4.6)); $\left[\lambda^{N}\right]$ is a $(N\times 6N)$ matrix; it is equal to: $\left[\lambda^{N}\right]=i\omega\left[q_j^{N}\right]$ (see Eq. (4.5)); the vectors $\left[\ddot{\xi}_{j0}^{N}\right]$, $\left[p_{in0}^{N}\right]$ are defined by Eqs. (6.3) and (6.6) and the vector $\left[q_D^{N}\right]$ by Eq. (4.5).

From Eq. (7.5) it can be obtained that the air pressure inside each OWC device is a function of the 6-degree displacement vector of each device of the array, i.e.

$$\left[p_{in0}^{N}\right]=\left[B^{N}\right]^{-1}\cdot\left[q_D^{N}\right]-\left[B^{N}\right]^{-1}\cdot\left[\lambda^{N}\right]\cdot\left[\ddot{\xi}_{j0}^{N}\right] \tag{7.6}$$

where $\left[B^{N}\right]^{-1}$ is the inverse matrix of $\left[B^{N}\right]$.

Substituting Eq. (7.6) into Eq. (7.4), the unknown motion components of each device can be calculated, each one being considered independently floating in the array.

8. Power absorption

The power absorbed, P^q, by each OWC device of the array, $q=1, \ldots, N$, can be written as (Falnes and McIver, 1985):

$$P^q=\frac{1}{2}\mathrm{Re}\left\{q^q\cdot\overline{\dot{p}_{in0}^{q}}\right\} \tag{8.1}$$

Here $\overline{\dot{p}_{in0}^{q}}$ is the complex conjugate of $\dot{p}_{in0}^{q}$. The term q^q for all the OWC devices of the array can be recast in a matrix form, see Eq. (4.5).

The capture efficiency, also called the relative capture width (Cruz, 2008) can be obtained by (Nader et al., 2012):

$$E_f^q=\frac{L_{pc}^{q}}{2b_q}=\frac{P^q}{2b_qP_w} \tag{8.2}$$

Here L_{pc}^{q} is the power capture width from the q device and P_w is the mean wave power (averaged over the wave period) per crest width of a monochromatic plane wave of amplitude $(H/2)$ and frequency ω:

$$P_w=\frac{1}{2}\rho g\left(\frac{H}{2}\right)^2C_g \tag{8.3}$$

where C_g is the group velocity.

The total capture efficiency by the array of N OWC devices can be obtained from Eq. (8.2), i.e. (Nader, 2013):

$$E_m = \frac{\frac{1}{N}\sum_{n=1}^{N} P^n}{2b_q P_w} = \frac{1}{N}\sum_{n=1}^{N} E_f^n \tag{8.4}$$

where P^n is the power absorbed by each OWC device of the array and E_f^n is the capture efficiency from each device defined by Eq. (8.1) and Eq. (8.2) respectively.

9. Time mean drift loads

By making use of the near-field method presented by Pinkster and Oortmerssen, 1977, the time-mean drift force and moment, acting on the device q of the array, can be obtained as:

$$\overrightarrow{F^{(2),q}} = -\int_{WL}\frac{1}{2}\rho\cdot g\cdot\overline{(\zeta_r^q)^2}\,\vec{n}\,dl + M\cdot\overrightarrow{R\cdot\ddot{X}_g^q} + \iint_{S_0^q}\frac{1}{2}\cdot\rho\cdot\overline{|\nabla\Phi^q|^2}\,\vec{n}\,dS + \iint_{S_0^q}\rho\cdot\overrightarrow{\dot{X}^q}\cdot\nabla\overrightarrow{\Phi_t^q}\,\vec{n}\,dS \tag{8.5}$$

Here the bars denote the time average; S_0^q, is the mean q device's wetted surface; ρ is the water density; g is the gravity acceleration; $\vec{n}$ is the unit normal vector pointing outwards to the device; M is the generalized mass matrix; $\overrightarrow{\dot{X}^q}$ is the vector of the first-order translations at a point on the device's wetted surface, which can be expressed as superposition of translation motions of the bodies' center of gravity, $\overrightarrow{\dot{X}_g^q}$, and the rotations around it. The latter are contained in the transformation matrix R (Mavrakos and Konispoliatis, 2012). The term $\overrightarrow{\ddot{X}_g^q}$, is the first-order translational accelerations of body's center of gravity and ζ_r^q, is the first-order relative wave elevation with respect to the transposed static water line WL on the q device. In Eq. (9.1), generalized normal vector components and mass moments of inertia have to be considered for evaluating the mean drift moments.

10. Numerical results

The calculation of the Fourier coefficients (see Section 3) is the most significant part of the numerical procedure, because of their influence on the accuracy of solution. For the case of the I and M ring element, $i=40$ terms were used, while for the III ring element $N=60$ terms; the number of interactions between the devices of the array were taken equal to 7 and the modes $m=\pm 7$, since it was found that the results obtained for those values were correct to an accuracy of within 1%. The presented results were obtained using the in house developed computer code HAMVAB (**H**ydrodynamic **A**nalysis of **M**ultiple **V**ertical **A**xisymmetric **B**odies, Mavrakos 1995) in FORTRAN programming language. The CPU time for each wave frequency related to the diffraction problem is about 6 s; while for the diffraction and motion radiation problem about 40 seconds and for the overall problem solution (diffraction, motion- and pressure- radiation problem) about 48 s.

Three different array configurations were examined. A three OWC array with the devices placed at the vertices of an equilateral triangle as shown in Fig. 2; and two different four-OWC arrays with the devices placed at the tops of a square with varying wall thicknesses (see Fig. 2). All devices in an array have the same dimensions. For the first two configurations, dimensionless parameters defining the system were selected as follows: $b/d=0{,}2$; $a/d=0{,}206$; $(d-h)/d=0{,}2$; whereas for the third configuration same as above but with $a/d=0{,}25$. The distance between two devices in the same row/column was L.

The investigated arrays are exposed to the action of regular monochromatic wave train propagating along the positive x-axis. As already mentioned in Section 4, the air compressibility in the chamber is neglected, thus the pneumatic admittance Λ^q is a real number. Its value for all the restrained OWCs was considered equal to the optimum coefficient Λ_{opt} of the same restrained OWC device but in isolation condition as in Evans and Porter (1996) work. As far as the freely floating OWCs is concerned, Λ^q was considered equal to the optimum coefficient Λ_{opt} of the same free floating OWC device but in isolation condition (Nader, 2013).

Before presenting the results obtained from the numerical model, we shall introduce the non-dimensional parameters of interest.

The exciting wave forces and moments acting on the first device of each OWC's array (see Fig. 2), $f_{i,1}, i=1,3,5$, are defined

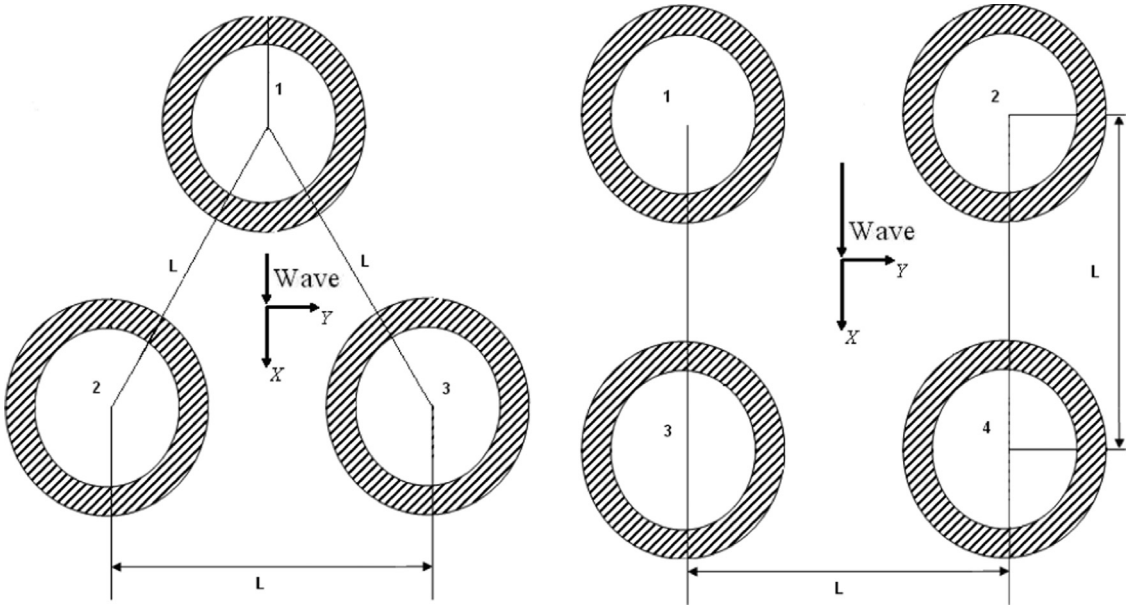

Fig. 2. Schematic representation of an array of three-and four-OWC devices.

as:

$$(f_{1,1},f_{3,1},f_{5,1}) = \left(\frac{f_x^1}{\rho g a^2 (H/2)},\frac{f_z^1}{\rho g a^2 (H/2)},\frac{M_y^1}{\rho g a^3 (H/2)}\right) \tag{10.1}$$

The modulus of the diffraction volume flow q_D^q in the first device of each configuration is made non-dimensional as:

$$\Gamma_D = \frac{|g_D^q|}{\omega S_i (H/2)}, for\ \ q=1 \tag{10.2}$$

The radiation conductance and the radiation susceptance in the first device of the array due to unit time harmonic oscillating pressure head inside the p-th device of each configuration ($p=1,2,3$ for triangle and $p=1,2,3,4$ for rectangular arrangement) have been made non-dimensional as:

$$(A_{1p},B_{1p}) = \left(\frac{g_p^{1p}}{b/(\rho\omega)},\frac{f_p^{1p}}{b/(\rho\omega)}\right) \tag{10.3}$$

where g_p^{qp}, f_p^{qp} are given by Eq. (4.3).

The total volume flow q^q, for the first device of each configuration has been presented as:

$$P_q = \frac{q^q}{\omega S_i (H/2)}, for\ \ q=1 \tag{10.4}$$

Here q^q is given in Eq. (4.2).

The total mean efficiency E_m, is obtained accordingly by:

$$E_m = \frac{1}{N}\sum_{n=1}^{N} E_{f,n} \tag{10.5}$$

where $E_{f,n}$ is the coefficient as calculated in Eq. (8.4).

The non-dimensional horizontal- and vertical-displacements and the pitch rotation of the first device, (x_1,x_3,x_5), in each array are defined by:

$$(x_1,x_3,x_5) = \left(\frac{\xi_{10}^q}{H/2},\frac{\xi_{30}^q}{H/2},\frac{\xi_{50}^q}{k\cdot H/2}\right), for\ \ q=1 \tag{10.6}$$

here $(\xi_{10}^q,\xi_{30}^q,\xi_{50}^q)$ are the motion components of the first device of the array when it is floating independently, as solution of Eqs. (7.5) and (7.4).

The horizontal mean second-order wave drift force, $f^{(2)}$, acting on the first device of each OWC array has been made non-dimensional as:

$$f^{(2)} = \frac{\overline{F_i^{(2),q}}}{\rho g a (H/2)^2}, q=1\ \ and\ \ i=x,y \tag{10.7}$$

where $\overline{F_i^{(2),q}}$ is evaluated by Eq. (9.1).

In Tables 1 and 2 the module of the exciting forces as defined by Eq. (10.1) are presented versus kd for the first OWC device of the first two configurations (see Fig. 2) for various distances between the devices over a frequency range of $1 \le kd \le 6$. It can be seen that for both configurations (three-and four-array arrangements) and for various distances between the OWCs, the vertical exciting force acting on the first OWC device has a peculiar behavior near $kd =$ 3,155, same as for the single isolated device. In the vicinity of $kd = 3{,}155$a resonance of the confined fluid inside the circular area of the device's chamber occurs. This peculiar behavior is typical for structures with moon pools. The fundamental hydrodynamic properties of such structures have been investigated some time ago (Garrett, 1970; Newman, 1977b). When a structure of this type is held fixed in incident monochromatic waves, the amplitude of the fluid motion will have local maxima at certain frequencies of the forcing. At these resonance frequencies, the magnitude of the exciting wave forces display also local maxima (see Tables 1 and 2). It should be mentioned that these resonances are annulled when the body is free to move (McIver, 2005).

Furthermore, as it can be seen from Tables 1 and 2, the hydrodynamic interactions between the OWCs affect the values of the exciting forces and moments, in dependence from the spacing between the devices. More specifically, the horizontal exciting forces and moments for the first device of both configurations attain a maximum value for spacing equals to $L=2a+b$. On the other hand, the maximum value of the vertical exciting force at the second arrangement is reached for $L=2a+5b$ while for the first configuration for spacing $L=2a+b,\ \ 2a+2b$.

In Figs 3 and 4 the modulus of the diffraction air volume flow as defined by Eq. (10.2) is given for the first OWC device in the first and second configuration, respectively, plotted versus kd for various distances among the devices. It is depicted that the dimensionless air volume flow of the diffraction problem in the first device of the first configuration remains unaffected by the spacing between the devices. The incoming wave firstly interacts with the first device and then with the remaining OWCs. On the other hand, in the second configuration the incoming wave firstly interacts with both first and second OWCs (see Fig. 2) and then with the remaining OWCs leading to different values of diffraction air volume flow especially in the neighborhood of their maximum attainable value which is reached for $L=2a+5b$.

In Fig. 5, the modulus of the diffraction air volume flow inside the first OWC device in the third configuration is plotted versus kd. Here, the dimensionless diffraction air volume flow is compared very well with Nader et al. (2014) results, who used a 3D finite element model in order to solve the diffraction and pressure radiation problem for an array of fixed OWCs.

In Figs. 6–13 the radiation conductance and the susceptance as defined by Eq. (10.3) are given for the first OWC device in the first and second configuration, respectively, plotted versus kd for various distances between the devices, whereas in Figs. 14–16 the radiation conductance and susceptance for the same OWC device as above for the third configuration is shown. In Figs. 6 and 9 the

Table 1
Modulus of the exciting wave forces and moments on the first OWC device of the first configuration for various kd compared to the corresponding ones of the single OWC device in isolation.

kd	$L=2a+b$			$L=2a+2b$			$L=2a+5b$			$L=2a+10b$			Isolated OWC		
	$f_{1,1}$	$f_{3,1}$	$f_{5,1}$	$f_{1,1}$	$f_{3,1}$	$f_{5,1}$	$f_{1,1}$	$f_{3,1}$	$f_{5,1}$	$f_{1,1}$	$f_{3,1}$	$f_{5,1}$	f_1	f_3	f_5
1.214	0.776	0.153	0.301	0.806	0.153	0.313	0.833	0.149	0.323	0.852	0.145	0.330	0.83	0.14	0.32
1.942	1.196	0.140	0.456	1.265	0.134	0.482	1.365	0.121	0.519	1.258	0.133	0.479	1.30	0.13	0.49
2.184	1.356	0.136	0.514	1.445	0.127	0.547	1.511	0.118	0.572	1.439	0.126	0.544	1.44	0.12	0.54
2.913	1.806	0.128	0.673	1.732	0.142	0,643	1.900	0.135	0.706	1.853	0.139	0.688	1.82	0.14	0.67
3.155	1.420	0.189	0.526	1.467	0.208	0.541	2.397	0.121	0.885	2.176	0.139	0.803	1.91	0.16	0.71
3.883	2.193	0.016	0.790	4.061	0.004	1.471	1.882	0.013	0.682	2.773	0.009	1.005	2.11	0.01	0.76
4.126	4.071	0.011	1.460	2.946	0.005	1.060	2.583	0.006	0.930	2.927	0.004	1.054	2.14	0.01	0.77
4.854	4.043	0.008	1.424	1.967	0.024	0.694	2.714	0.015	0.959	1.526	0.026	0.539	2.15	0.02	0.76
5.097	3.324	0.016	1.163	1.687	0.027	0.592	2.416	0.019	0.847	2.100	0.023	0.737	2.13	0.02	0.74

Table 2
Modulus of the exciting wave forces and moments on the first OWC device of the second configuration for various kd compared to the corresponding ones of the single OWC device in isolation.

kd	$L=2a+b$			$L=2a+2b$			$L=2a+5b$			$L=2a+10b$			Isolated OWC		
	$f_{1,1}$	$f_{3,1}$	$f_{5,1}$	$f_{1,1}$	$f_{3,1}$	$f_{5,1}$	$f_{1,1}$	$f_{3,1}$	$f_{5,1}$	$f_{1,1}$	$f_{3,1}$	$f_{5,1}$	f_1	f_3	f_5
1.214	0.817	0.153	0.317	0.827	0.152	0.320	0.844	0.148	0.327	0.844	0.146	0.327	0.83	0.14	0.32
1.942	1.292	0.137	0.492	1.330	0.130	0.506	1.340	0.123	0.510	1.293	0.128	0.492	1.30	0.13	0.49
2.184	1.480	0.131	0.560	1.520	0.121	0.575	1.446	0.123	0.547	1.478	0.123	0.559	1.44	0.12	0.54
2.913	1.820	0.124	0.677	1.768	0.129	0.657	1.802	0.144	0.669	1.828	0.140	0.679	1.82	0.14	0.67
3.155	1.518	0.156	0.560	1.865	0.146	0.688	1.752	0.221	0.647	1.923	0.145	0.710	1.91	0.16	0.71
3.883	3.094	0.011	1.118	2.410	0.013	0.873	2.558	0.007	0.927	2.486	0.010	0.901	2.11	0.01	0.76
4.126	3.585	0.002	1.288	2.274	0.009	0.819	2.572	0.005	0.926	2.343	0.006	0.844	2.14	0.01	0.77
4.854	2.498	0.025	0.881	1.432	0.028	0.505	2.057	0.018	0.727	2.241	0.018	0.791	2.15	0.02	0.76
5.097	2.466	0.025	0.864	1.365	0.027	0.479	1.963	0.020	0.689	2.654	0.013	0.931	2.13	0.02	0.74

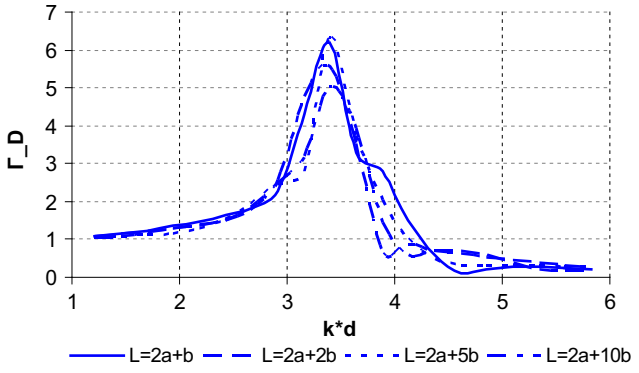

Fig. 3. Modulus of the diffraction volume flow, Γ_D, in the first OWC of the first configuration versus kd.

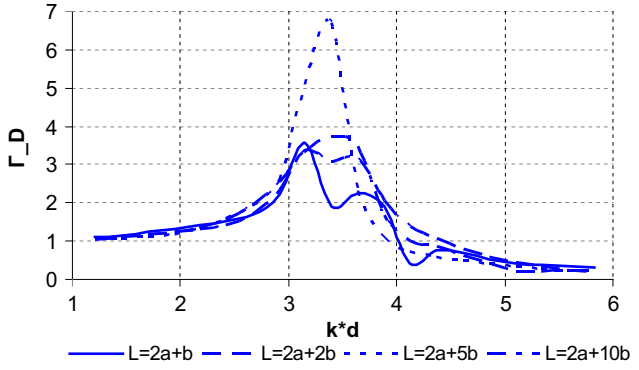

Fig. 4. Modulus of the diffraction volume flow, Γ_D, in the first OWC of the second configuration versus *kd*.

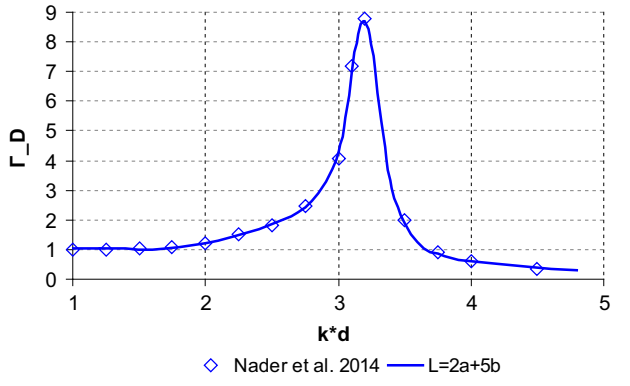

Fig. 5. Modulus of the diffraction volume flow, Γ_D, in the first OWC of the third configuration versus *kd* compared with Nader et al. (2014) results.

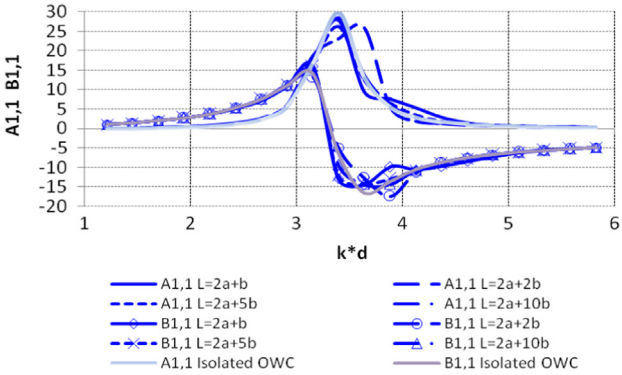

Fig. 6. Radiation conductance and susceptance $(A_{1,1}, B_{1,1})$ for the first OWC device of the first configuration versus *kd* compared to the corresponding ones of the single OWC device in isolation.

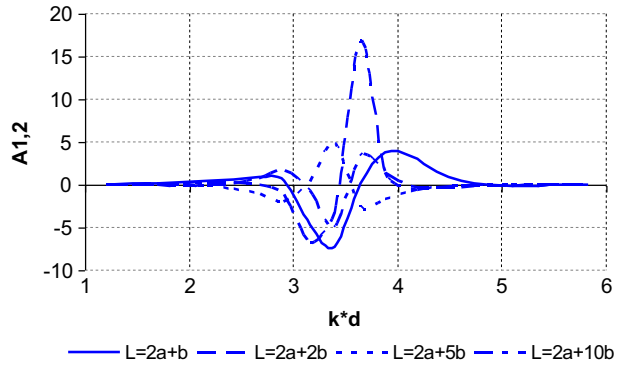

Fig. 7. Radiation conductance $A_{1,2}$ for the first OWC device of the first configuration versus kd.

radiation conductance and susceptance for the first device of both configurations due to its own pressure head are fairly similar compared to those for the isolated OWC. Moreover, same as in the discussion of Fig. 3, in the triangular OWC arrangement the radiation conductance and susceptance values remain unaffected by the spacing between the devices contrary to those obtained in the rectangular configuration in which they attain different values especially for $3 \leq kd \leq 4$.

In addition, from Figs 7,8 and 10–13 it is observed that the radiation conductances A_{12}, A_{14} and susceptances B_{12}, B_{14} in the first device due to pressure variation in the second and the forth device of the arrangement, respectively, exhibit non-negligible values, and hence, the radiated wave induced by the inner pressure of the rest of the OWCs in the array seems to have significant importance in the solution of the hydrodynamic problem. As expected, due to symmetry reasons, the radiation conductance

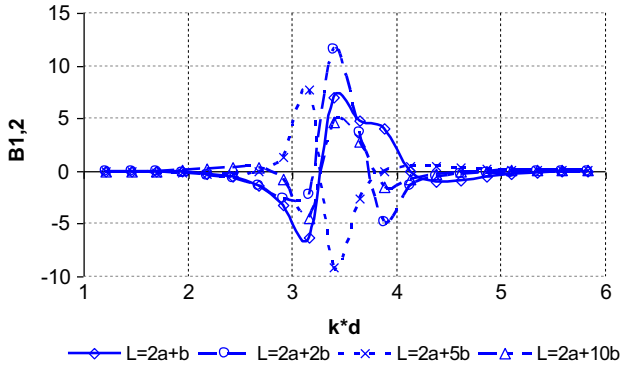

Fig. 8. Radiation susceptance $B_{1,2}$ for the first OWC device of the first configuration versus kd.

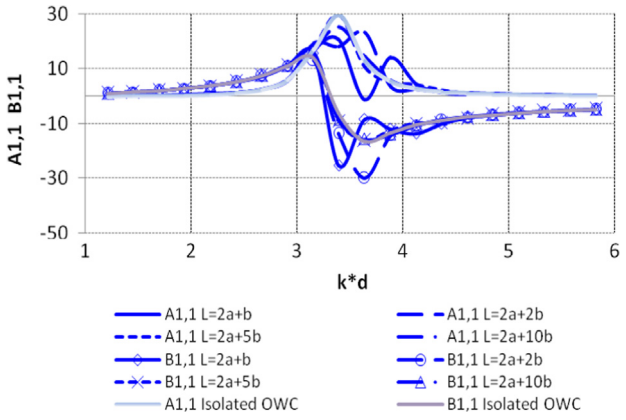

Fig. 9. Radiation conductance and susceptance $(A_{1,1}, B_{1,1})$ for the first OWC device of the second configuration versus kd compared to the corresponding ones of the single OWC device in isolation.

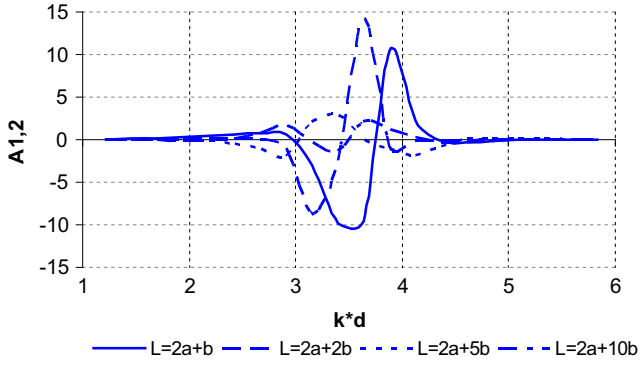

Fig. 10. Radiation conductance $A_{1,2}$ for the first OWC device of the second configuration versus kd.

and susceptance for the first OWC due to air pressure inside the second device (see Fig. 2) equal to those for the first OWC due to air pressure inside the third OWC, i.e. $A_{12}=A_{13}$ and $A_{13}=B_{13}$. In Figs. 14–16 the radiation conductance and susceptance for the first device in the third configuration is plotted against Nader et al. (2014) results. Comparing the results from the above Figs. 6–16 it becomes evident that the radiated waves from each device of the array are dependent on the relative position of the OWCs in the array and on the geometrical characteristics (i.e. thickness of the oscillating chamber) of each OWC.

In order to justify the number of interactions (i.e. 7) used in the solution process, the values of: $N\_A_{12}=(A^i_{12}-A^1_{12})/A^1_{12}$, $N\_B_{12}=(B^i_{12}-B^1_{12})/B^1_{12} N\_A_{14}=(A^i_{14}-A^1_{14})/A^1_{14}$ and $N\_B_{14}=(B^i_{14}-B^1_{14})/B^1_{14}$ are presented in Fig. 17–20 plotted against *kd* for

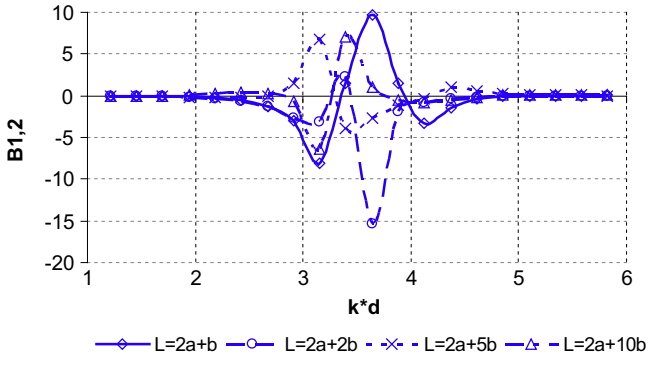

Fig. 11. Radiation susceptance $B_{1,2}$ for the first OWC device of the second configuration versus *kd*.

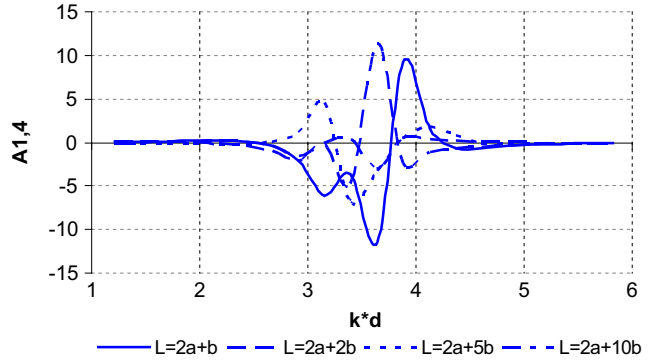

Fig. 12. Radiation conductance $A_{1,4}$ for the first OWC device of the second configuration versus kd.

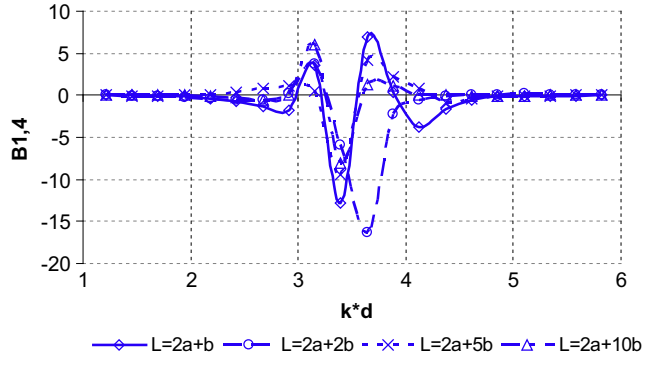

Fig. 13. Radiation susceptance $B_{1,4}$ for the first OWC device of the second configuration versus *kd*.

progressive increase of the number of interactions considered. Here A^i_{12}, A^i_{12} and B^i_{12},B^i_{12} as defined by Eq. (10.3) denote the radiation conductance and susceptance, respectively, for the *i-th* interaction order, of the third configuration ($i=1,..,7$), whereas A^1_{12}, A^1_{12},B^1_{12},B^1_{12} denote the radiation conductance and susceptance, respectively, for the first order of interaction between the devices. It becomes clear that outside the neighborhood of the radiation conductance and susceptance maximum attainable value (i.e. $kd=1,2$) a couple of interactions are enough to describe accurately the multiple scattering formulation. On the other hand in the neighborhood of their maximum attainable value (i.e. $kd=2,4$, $kd=4$), seven (7) interaction orders seem to be the lower limit in order to receive accurate results.

In Figs. 21 and 22 the modulus of the non–dimensional total volume flow P_1, as defined by Eq. (10.4), is plotted versus *kd* in the first device of the first and second array configurations for

different spacing between the devices, the latter being considered restrained in the incident wave train. In Figs. 23 and 24 the modulus of the non-dimensional total volume flow P_1, versus kd in the first device of the first and third array configurations are presented when the devices are freely floating. The mass moment of inertia with respect to the center of gravity of each OWC device is derived from

$$I=\rho_w\nabla\left(b_q+\frac{a_q-b_q}{2}\right)^2 \tag{10.8}$$

Here ∇ denotes the volume of each OWC device, ρ_w the water density and $a_q, b_q (q=1,..,N)$ the outer and inner radii of each device as defined above.

From Figs. 21 and 22 it is depicted that as the spacing between the OWC devices is increasing the total volume flow in the first device tends to the one corresponding to an OWC in isolation condition since the interaction phenomena between the devices decrease significantly. In addition, as far as the rectangular arrangement is concerned, it can be seen that the total air volume

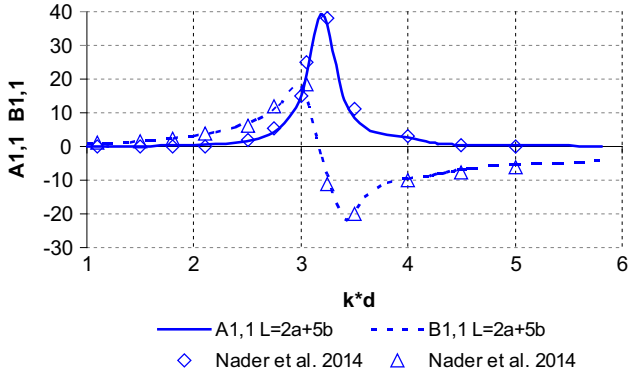

Fig. 14. Radiation conductance and susceptance $(A_{1,1}, B_{1,1})$ for the first OWC device of the third configuration versus kd compared with Nader et al. (2014) results.

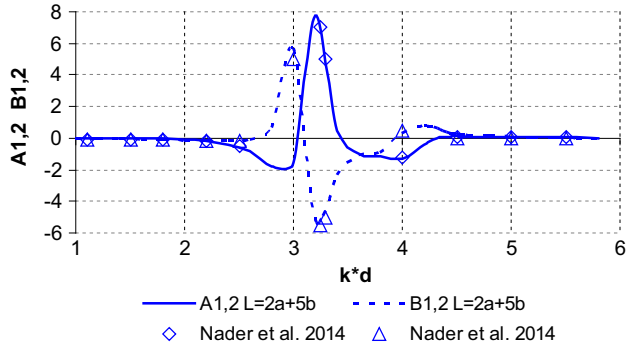

Fig. 15. Radiation conductance and susceptance $(A_{1,2}, B_{1,2})$ for the first OWC device of the third configuration versus kd compared with Nader et al. (2014) results.

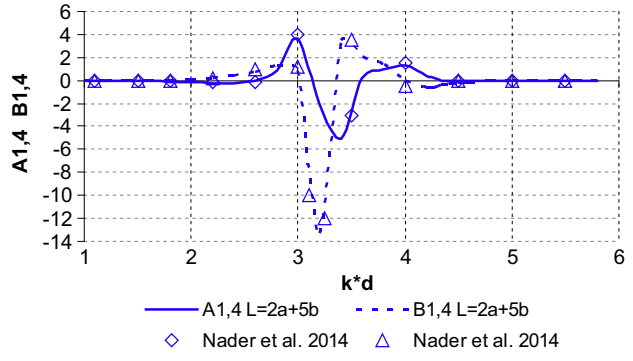

Fig. 16. Radiation conductance and susceptance $(A_{1,4}, B_{1,4})$ for the first OWC device of the third configuration versus kd compared with Nader et al. (2014) results.

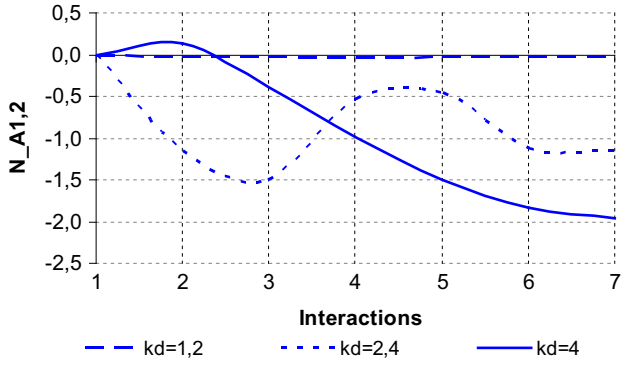

Fig. 17. Graphics for $N\_A_{1,2}$ versus N interactions.

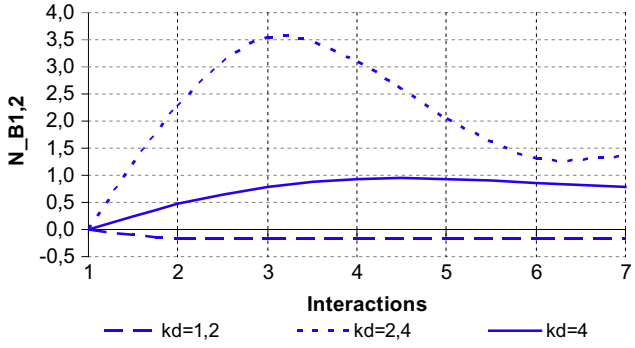

Fig. 18. Graphics for $N\_B_{1,2}$ versus N interactions.

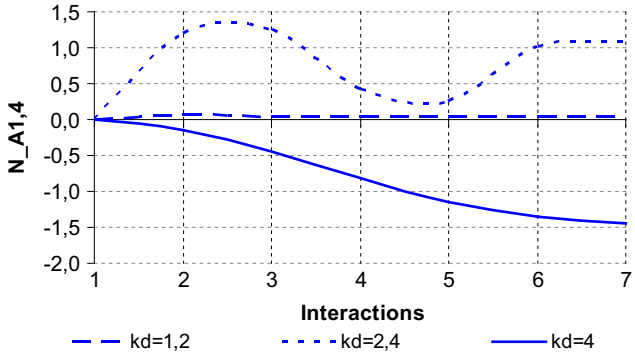

Fig. 19. Graphics for $N\_A_{1,4}$ versus N interactions.

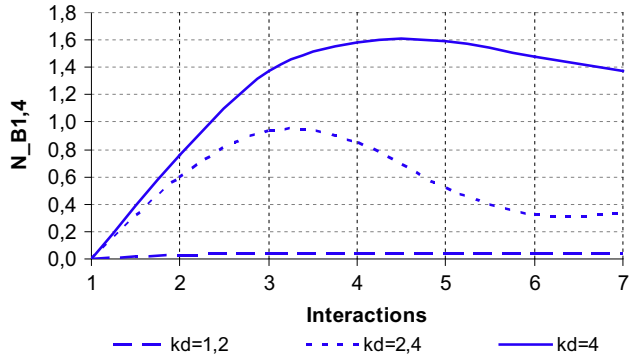

Fig. 20. Graphics for $N\_B_{1,4}$ versus N interactions.

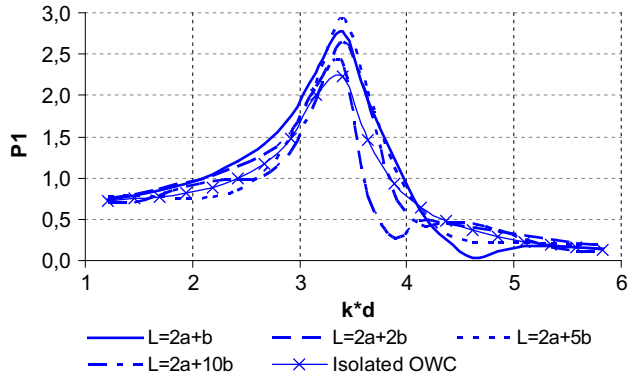

Fig. 21. Modulus of the total volume flow, P_1, in the first OWC of the first configuration for restrained OWC devices versus kd compared with the total volume flow in the single OWC device in isolation.

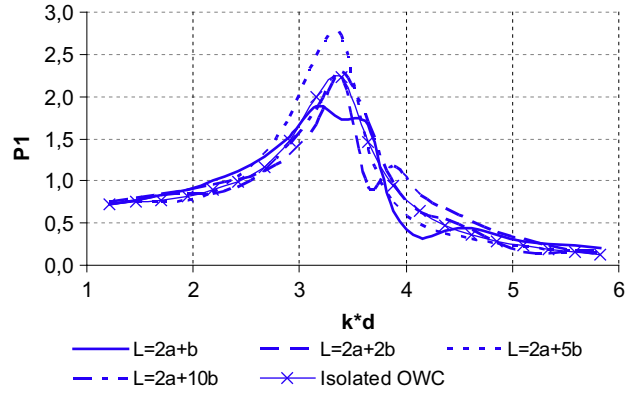

Fig. 22. Modulus of the total volume flow, P_1, in the first OWC of the second configuration for restrained OWC devices versus kd compared with the total volume flow in the single OWC device in isolation.

flows show significant variations compared to the corresponding ones of the triangular configuration, especially near their maximum attainable values for varying spacing.

Next, form Fig. 23 it is evident that the total air volume flow for the free floating devices is lower than the one corresponding to the restrained devices (Fig. 21) except near $kd=4,8$. The same evidence was found when the inner air pressure head in a single isolated restrained device was compared to its freely floating counterpart (Mavrakos and Konispoliatis, 2012). In Fig. 24 the total volume flow inside the first device of the array is compared to the one of a single free floating OWC device with same geometrical characteristics as the ones investigated by Nader (2013). The frequencies $kd=4,8$ (see Fig. 23) and $kd=4,5$(see Fig. 24) where the peak values of the air volume flow are obtained, correspond to the natural resonance frequencies of the heave motion of the device for each configuration.

The total mean efficiency E_m, as defined by Eq. (10.5), in the first two arrangements for varying spacing between their OWC's devices is presented in Figs. 25–28 for a frequency range of $1\leq kd\leq 6$. More specifically, in Figs. 25 and 27 the mean efficiency of the OWCs in the first configuration is given, when the devices are considered either restrained in incident regular waves (Fig. 25) or freely floating (Fig. 27). In Fig. 26 the results of the present method are compared with the ones of Nader et al. (2012), when the devices are considered restrained in regular waves. In Fig. 28 the mean efficiency for the free independently floating array of four OWCs (second configuration) is being plotted.

The overall maximum mean efficiency for both three and four restrained OWC's arrays configurations is attained near $kd=3,4$ for spacing equal to $L=2a+5b$. This peak efficiency for the restrained four OWC's array configuration is up to 20% higher than the peak efficiency attained by the same restrained OWC in isolation condition, while for the restrained three OWCs is up to 3% higher for restrained isolated OWC. On the other hand, for both three and four free floating OWC's arrays configurations two different peak values are presented. Firstly, near $kd=3,4$ where as mentioned above the overall maximum mean efficiency is for spacing equal to $L=2a+5b$ and secondly, at the resonance frequency of the heaving motion of the device where $L=2a+5b$ has the worst performance of all spacing values.

From the above depicted results it is observed that an increase of the wave interaction effects (for example by lowering the spacing among the devices) does not necessarily leads to an increase of the absorbed energy by the devices. Babarit et al. (2010) arrived to the same conclusion examining an array of two WEC devices in regular and irregular wave impact. Following the remarks by Nader et al. (2012), the arrays of OWC devices can be divided into three broad categories, depending from the non-dimensional ratio of the wavelength to the inter-body spacing in the array. The first category is where the distance between the devices is lower than the wavelength. In this case the arrangement behaves as a larger, single OWC device. The second category is when the spacing between the devices has a very large value compared with λ. In this case the interaction phenomena between the devices decrease significantly and each device tends to behave as an OWC in isolation condition. The third category is when the value of the spacing between the OWCs tends to λ. In the present case of the three- and four-device configurations, the distance $L=2a+5b$ belongs to this category, as the wave length approximates to $1,85d$ and the distance $L=1,412d$ for the particular geometry. Thus, the

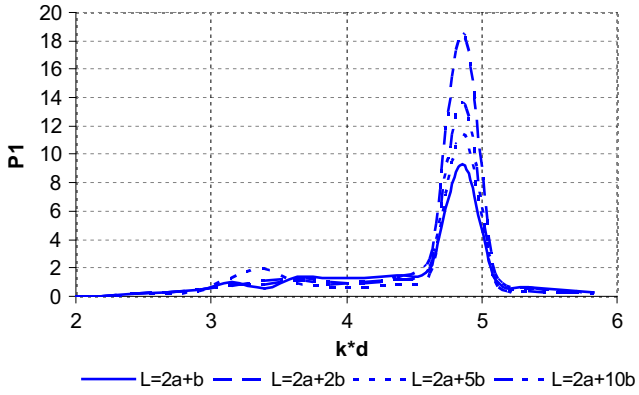

Fig. 23. Modulus of the total volume flow, P_1, in the first OWC of the first configuration for free floating OWC devices versus kd.

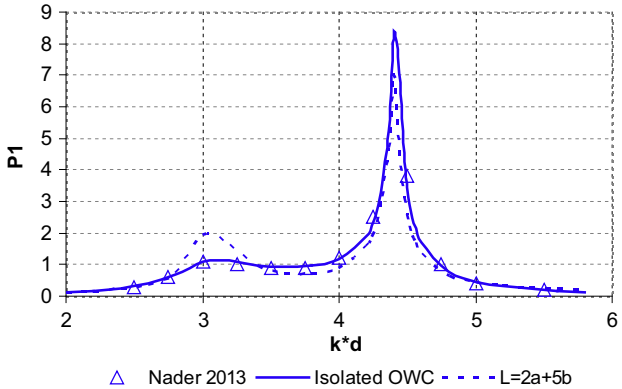

Fig. 24. Modulus of the total volume flow, P_1, in the first OWC of the third configuration for free floating OWC devices versus kd compared with the total volume flow in the single OWC device in isolation and with Nader (2013) results.

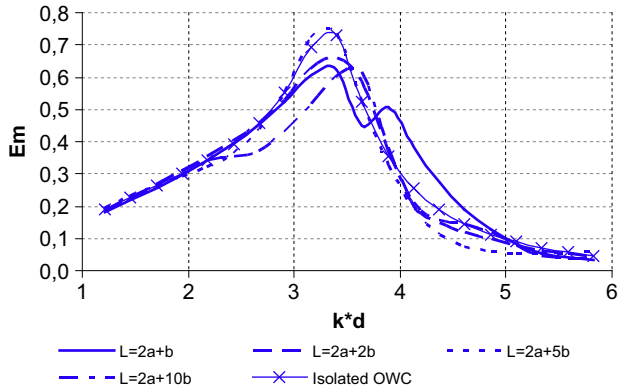

Fig. 25. Total mean efficiency, E_m, versus kd for the first configuration of OWC devices restrained in regular waves for various spacing's among the devices compared with the efficiency of the single OWC device in isolation.

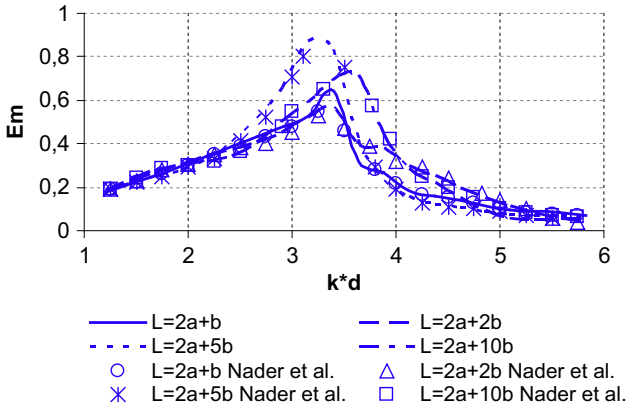

Fig. 26. Total mean efficiency, E_m, versus kd for the second configuration of OWC devices restrained in regular waves for various spacing's among the devices compared with the efficiency of the single OWC device in isolation and with the Nader et al. (2012) results.

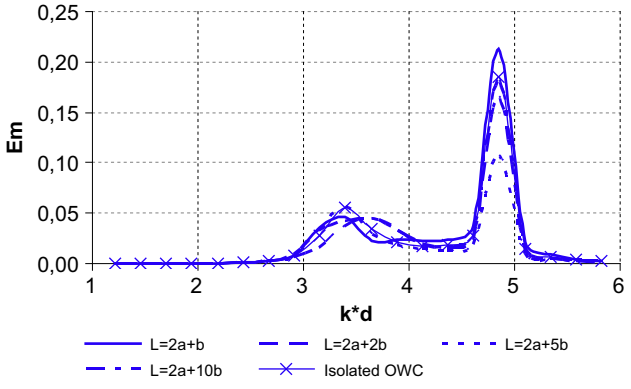

Fig. 27. Total mean efficiency,E_m, versus kd for the first configuration of free floating OWC devices for various spacing among the devices, compared with the efficiency of the single OWC device in isolation.

selection of the array spacing can significantly enhance the total power output.

In Figs. 29–31 the non–dimensional translational and rotational motions, as defined by Eq. (10.6), of the first OWC device in the first two arrangements (see Fig. 2), are plotted for various spacing and for a frequency range of $1 \leq kd \leq 6$. It can be noticed that the horizontal surge motions (Fig. 29) and the pitch rotations (Fig. 31)

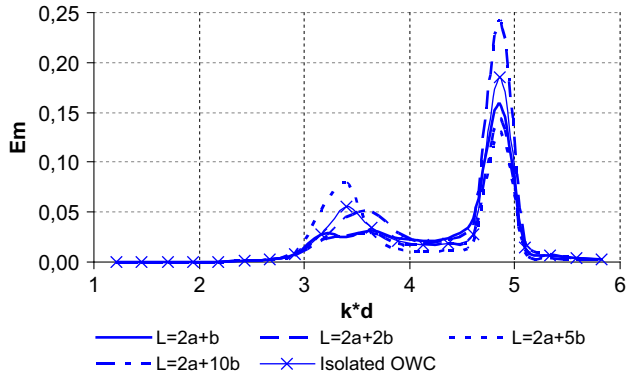

Fig. 28. Total mean efficiency,E_m, versus kd for the second configuration of free floating OWC devices for various spacing among the devices, compared with the efficiency of the single OWC device in isolation.

in both arrangements differ a lot from the ones obtained from the same OWC device in isolation. These differences can be traced back to the hydrodynamic interaction phenomena among the devices and the oscillating air pressure head inside each device of the array, since for the isolated device there are no hydrodynamic interactions and the inner air pressure do not affect the horizontal motion and rotation (Mavrakos and Konispoliatis, 2012). As far as the heave motion (Fig. 30) of the first OWC is concerned, its maximum value is attained for $kd=3{,}4$ and 4,8, i.e. at the same kd values as the mean efficiency (Figs. 27 and 28). For $kd=3{,}4$ the vertical displacement of the OWC for both the three- and four-array configurations reaches a maximum value for spacing $L=2a+5b$. At $kd=4{,}8$ the heave resonances of the floating OWC's occur for all the inter-body spacing. For the frequencies outside the neighborhood of $kd=3{,}4$ and $kd=4{,}8$ the different arrays layouts (triangle or rectangular) seem to have little effect on the vertical displacement of the first OWC for all the examined spacing. Moreover, as far as the resonances of the water motion occurred inside the restrained OWC's with the internal moon pool and the associated peaks of the heave exciting forces on the devices (see results included in Tables 1 and 2) when they are exposed to the action of surface regular waves are annulled when the devices are freely floating (McIver, 2005; Mavrakos and Katsaounis, 2010). Hence, even in their neighborhood of occurrence, they do not affect the motion of the free floating device, which is therefore dominated by any nearby motion resonance due to hydrostatic restoring force. In Fig. 30 the aforementioned annulment becomes evident as at its expected location of occurrence, that is, near $kd=3{,}155$ no peak in the heave response occurs. The kinematic behavior of the floating device is dominated by the existing motion resonance, which occurred near $kd=4,8$.

In Figs. 32 and 33 the horizontal drift forces acting on the first device in the first two configurations (see Fig. 2) along the x-axis are plotted for various spacing and for a frequency range of $1 \leq kd \leq 6$ (for definitions see Eq. (10.7)). The OWCs in Fig. 32 are considered restrained in incident regular waves while in Fig. 33 the devices are considered free floating. It can be noticed that the horizontal drift forces differ a lot between the two arrangements. These variations occur due to the number of OWCs which compose each arrangement and the hydrodynamic interaction phenomena among them. In Figs. 34 and 35 the horizontal drift forces acting on the same as above OWC device for the second configuration along the y-axis are presented. As it was expected the horizontal drift forces on the first OWC along the y-axis for the first configuration equals to zero.

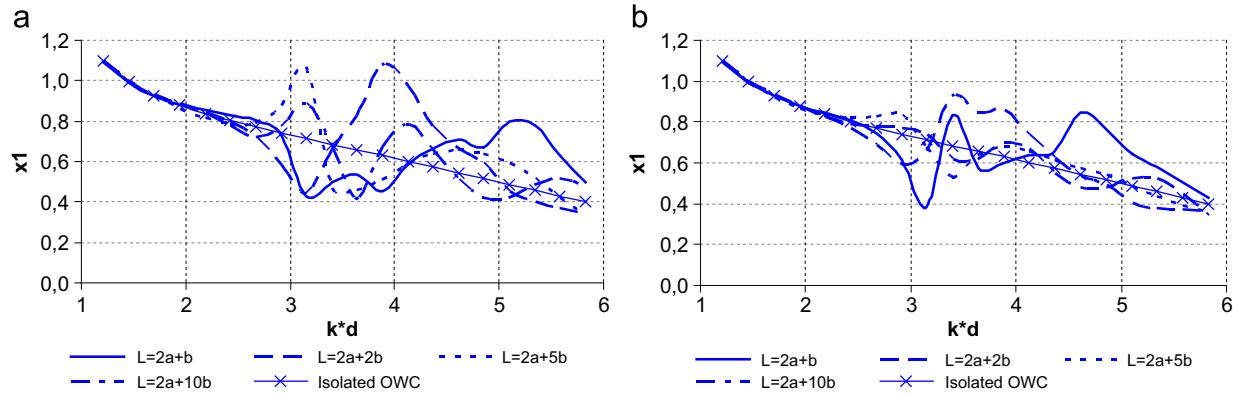

Fig. 29. Non-dimensional horizontal surge motion of the first OWC in the first (a) and the second (b) arrangement for various spacing values versus *kd*, compared to the corresponding displacement of the single OWC in isolation.

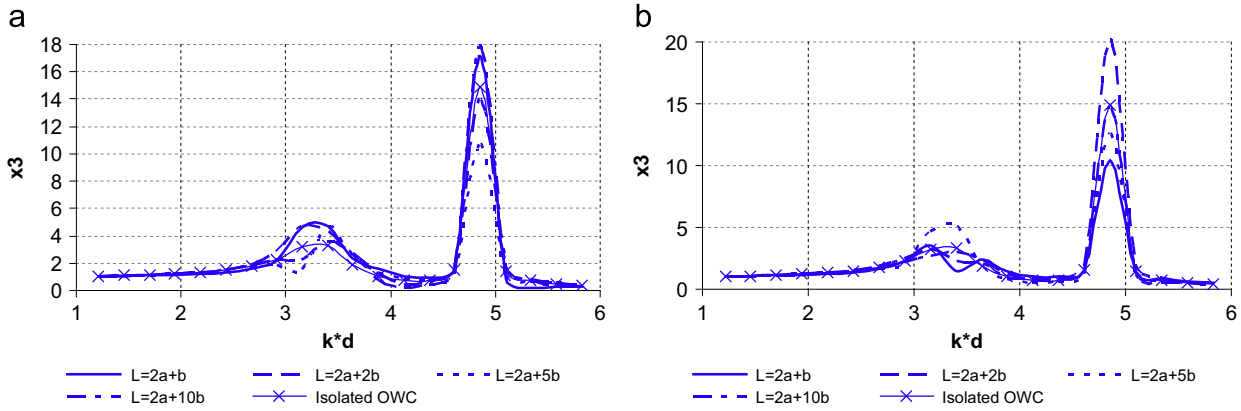

Fig. 30. Non-dimensional heave motion of the first OWC in the first (a) and the second (b) arrangement for various spacing values versus *kd*, compared to the corresponding displacement of the single OWC in isolation.

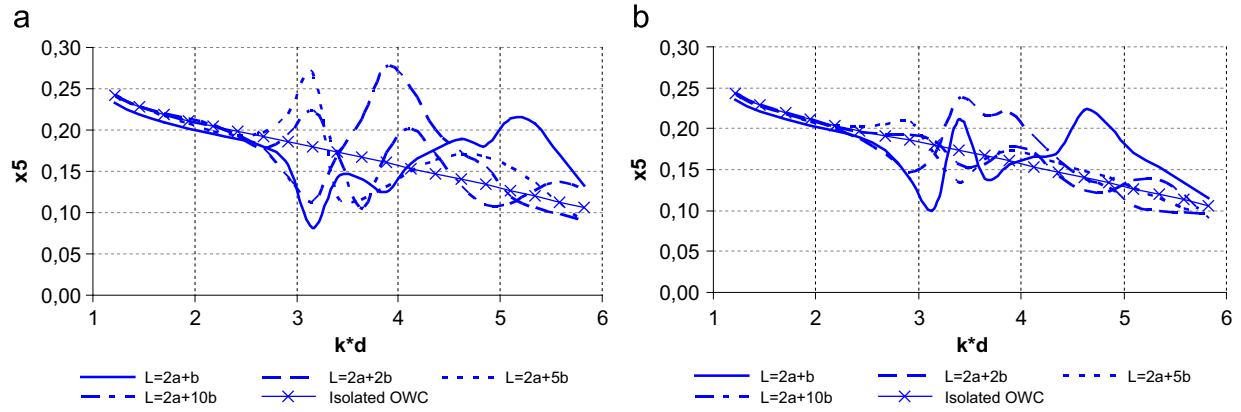

Fig. 31. Non–dimensional pitch motion of the first OWC in the first (a) and the second (b) arrangement for various spacing values versus *kd*, compared to the corresponding pitch motion of the single OWC in isolation.

11. Conclusion

An analytical method has been developed to solve the diffraction, the motion– and pressure-dependent radiation problems around an array of vertical axisymmetric OWC devices. This method provides an efficient tool for complete hydrodynamic analysis of these devices, including the evaluation of the first- and mean-second order wave forces, the pressure hydrodynamic parameters and the power efficiency.

The depicted results indicate that the radiated waves from each OWC device are affected by the distance between the devices in an array. Major improvements have been demonstrated for an array spacing of $L=2a+5b$ either restrained or free floating. Moreover, the coupling between the number of the OWCs in the array and their placement against the wave front may affect significantly the power capture efficiency. Finally, the presented results demonstrate that the interaction phenomena between the OWCs exhibit non-negligible effect on the mean second order forces. The

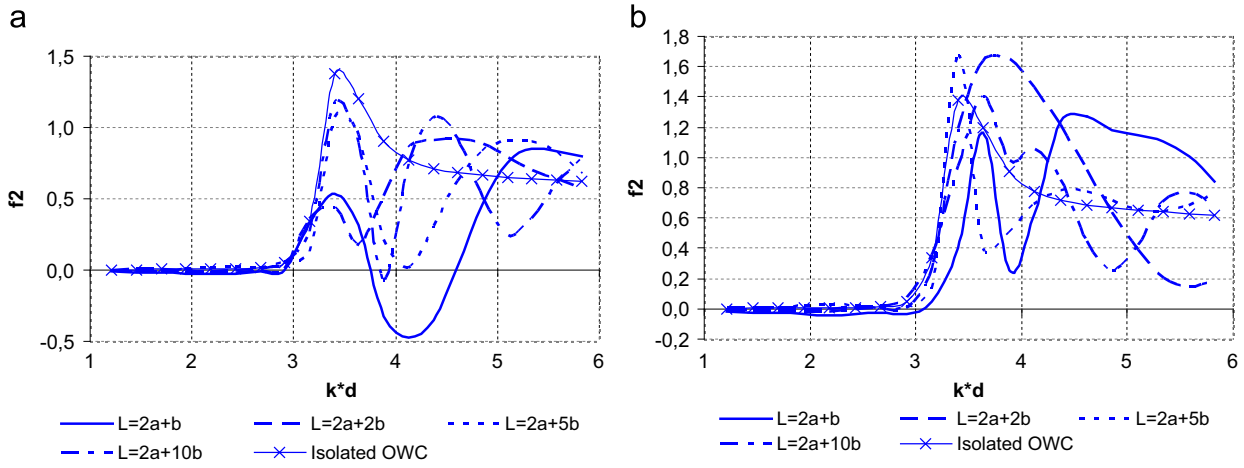

Fig. 32. Horizontal drift forces along the *x*-axis for various spacing versus *kd* for the first OWC of the first (a) and the second (b) arrangement of OWC devices restrained in regular waves, compared with the horizontal drift force on the single OWC device in isolation.

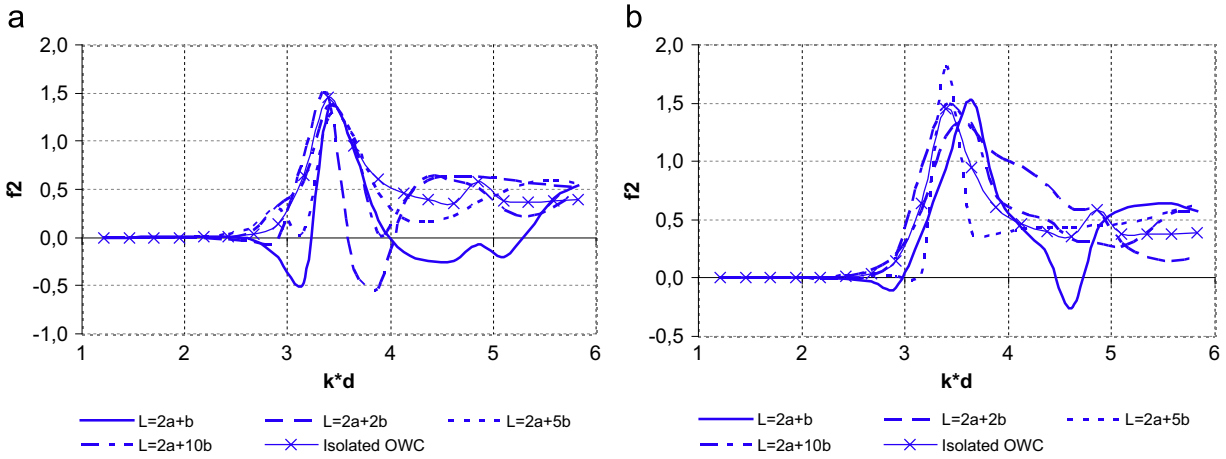

Fig. 33. Horizontal drift forces along the *x*-axis for various spacing versus *kd* for the first OWC of the first (a) and the second (b) arrangement of free floating OWC devices, compared with the horizontal drift force on the single OWC device in isolation.

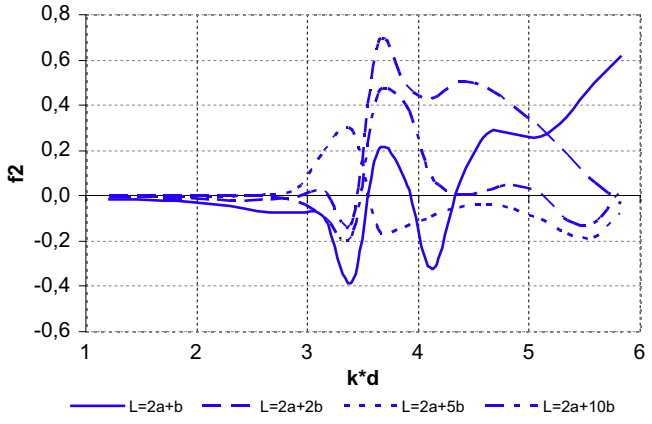

Fig. 34. Horizontal drift forces along the *y*-axis for various spacing versus *kd* for the first OWC of the second arrangement of OWC devices restrained in regular waves.

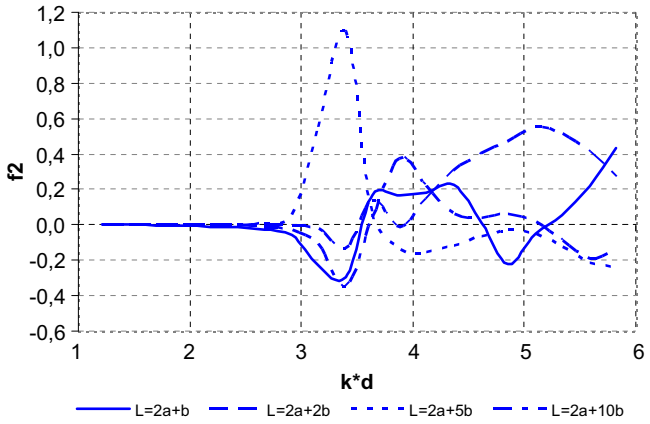

Fig. 35. Horizontal drift forces along the *y*-axis for various spacing versus *kd* for the first OWC of the second arrangement of free floating OWC devices.

importance of these load components is high since they may cause large body excursions from its mean position when the restoring forces are weak, although generally small in magnitude compared with their first–order oscillatory parts.

It could be interesting to study in further works how the power efficiency is influenced when the OWC devices are connected together forming an integrated floating platform. It might also be relevant to analyse different wave angles of the incident regular or irregular waves.

Acknowledgments

This research has been co-financed by the European Union (European Social Fund– ESF) and Greek National Funds through the Operational Program "Education and Lifelong Learning" of the National Strategic Reference Framework (NSRF) 2007–2013: Research Funding Program: ARISTEIA, Program POSEIDON (2041).

Appendix A

The total velocity potential, obtained from the solution of the pressure-radiation problem, for the *III* fluid domain ($b_q \le r_q \le a_q, 0 \le z \le h_q$) can be written as:

$$\phi_P^{III,qp}(r_q,\theta_q,z) = -i\frac{1}{\omega\rho}\sum_{m=-\infty}^{\infty}\left[\sum_{n=0}^{\infty}\varepsilon_n\left[\left(F_{P,m,n}^{III,qp}+\delta_{q,p}F_{P,0,n}^{III,p}\right)R_{mn}^{III} + \left(F_{P,m,n}^{*III,qp}+\delta_{q,p}F_{P,0,n}^{*III,p}\right)R_{mn}^{*III}\right]\cos\left(\frac{n\pi z}{h_q}\right)\right]\cdot e^{im\theta_q} \tag{A1}$$

where:

$$R_{mn}^{III}(r_q) = \frac{K_m(n\pi b_q/h_q)I_m(n\pi r_q/h_q) - I_m(n\pi b_q/h_q)K_m(n\pi r_q/h_q)}{I_m(n\pi a_q/h_q)K_m(n\pi b_q/h_q) - I_m(n\pi b_q/h_q)K_m(n\pi a_q/h_q)}, m,n \neq 0$$

$$R_{m0}^{III}(r_q) = \frac{(r_q/b_q)^m - (b_q/r_q)^m}{(a_q/b_q)^m - (b_q/a_q)^m}, \quad m \neq 0, n = 0 \quad R_{00}^{III}(r_q) = \frac{\ln(r_q/b_q)}{\ln(a_q/b_q)}, \quad m,n = 0$$

$$R_{mn}^{*\,III}(r_q) = \frac{I_m(n\pi a_q/h_q)K_m(n\pi r_q/h_q) - K_m(n\pi a_q/h_q)I_m(n\pi r_q/h_q)}{I_m(n\pi a_q/h_q)K_m(n\pi b_q/h_q) - I_m(n\pi b_q/h_q)K_m(n\pi a_q/h_q)}, m,n \neq 0$$

$$R_{m0}^{*III}(r_q) = \frac{(a_q/r_q)^m - (r_q/a_q)^m}{(a_q/b_q)^m - (b_q/a_q)^m}, \quad m \neq 0, n = 0 \quad R_{00}^{*III}(r) = \frac{\ln(a_q/r_q)}{\ln(a_q/b_q)}, \quad m,n = 0 \tag{A2}$$

and ε_n is the Neumann's symbol defined as: $\varepsilon_0 = 1$, for $n=0$; otherwise $\varepsilon_n = 2$.

For the *M* fluid domain ($0 \le r_q \le b_q, 0 \le z \le d$), the total velocity potential can be written as:

$$\phi_P^{M,qp}(r_q,\theta_q,z) = -i\frac{1}{\omega\rho}\left[\delta_{q,p}g_{P,0}^{M,p}(r_p,z) + \sum_{m=-\infty}^{\infty}\sum_{n=0}^{\infty}\left(F_{P,m,n}^{M,qp}+\delta_{q,p}F_{P,0,n}^{M,p}\right)\frac{I_m(\mathrm{a}_n r_q)}{I_m(\mathrm{a}_n b_q)}Z_n(z)\cdot e^{im\theta_q}\right] \tag{A3}$$

where $g_{P,0}^{M,p} = 1$

The orthonormal functions $Z_j(z)$ are defined by Eqs. (2.11), (2.17).

Appendix B

The defining equations for $L_{n,i}$ are Eqs. (3.5), (3.6), (3.7) and (3.8) where:

for $i \ge 1, \mathrm{a}_i \neq n\pi/h_q$, then:

$$L_{n,i} = \frac{1}{h_q}\int_0^{h_q} Z_i(z)\cos\left(\frac{n\pi z}{h_q}\right)dz = (-1)^n\left[\frac{1}{2}\left[1+\frac{\sin(2\mathrm{a}_i d)}{2\mathrm{a}_i d}\right]\right]^{-1/2}\frac{\mathrm{a}_i h_q}{\mathrm{a}_i^2 h_q^2 - n^2\pi^2}\sin(\mathrm{a}_i h_q) \tag{B1}$$

for $i = 0$, then:

$$L_{n,i} = \frac{1}{h_q}\int_0^{h_q} Z_0(z)\cos\left(\frac{n\pi z}{h_q}\right)dz = (-1)^n\left[\frac{1}{2}\left[1+\frac{\sinh(2kd)}{2kd}\right]\right]^{-1/2}\frac{kh_q}{k^2h_q^2 + n^2\pi^2}\sinh(kh_q) \tag{B2}$$

for $i \ge 1, \mathrm{a}_i = n\pi/h_q \neq 0$, then:

$$L_{n,i} = \frac{1}{h_q}\int_0^{h_q} Z_i(z)\cos\left(\frac{n\pi z}{h_q}\right)dz = \frac{1}{2}\left[\frac{1}{2}\left[1+\frac{\sin(2\mathrm{a}_i d)}{2\mathrm{a}_i d}\right]\right]^{-1/2} \tag{B3}$$

Value of $Q_{p,0,n}^*$:

$$Q_{p,0,n}^* = \frac{1}{h_q}\int_0^{h_q}\cos\left(\frac{n\pi z}{h_q}\right)dz = \begin{cases} 0, & n \neq 0 \\ 1, & n = 0 \end{cases} \tag{B4}$$

The defining equations for $A_{m,i}^M, D_{m,n}^{III,qp}, D_{m,n}^{*III,qp}, A_{m,i}^I, A_{m,n}^{III,qp}, A_{m,n}^{*III,qp}$ and $D_{m,i}^I$ are Eqs. (3.7) and (3.8) where:

$$A_{m,i}^M = \mathrm{a}_i b_q \left.\frac{\partial I_m(\mathrm{a}_i r_q)}{\partial r_q}\right|_{r=b_q}\frac{1}{I_m(\mathrm{a}_i b_q)} \tag{B5}$$

$$A_{m,i}^I = \mathrm{a}_i a_q \left.\frac{\partial K_m(\mathrm{a}_i r)}{\partial r}\right|_{r=a_q}\frac{1}{K_m(\mathrm{a}_i a_q)} \tag{B6}$$

$$D_{m,n}^{III,qp} = b_q\left.\frac{\partial R_{mn}^{III}}{\partial r}\right|_{r=b_q}, D_{m,n}^{*III,qp} = b_q\left.\frac{\partial R_{mn}^{*III}}{\partial r}\right|_{r=b_q} \tag{B7}$$

$$A_{m,n}^{III,qp} = a_q\left.\frac{\partial R_{mn}^{III}}{\partial r}\right|_{r=a_q}, A_{m,n}^{*III,qp} = a_q\left.\frac{\partial R_{mn}^{*III}}{\partial r}\right|_{r=a_q} \tag{B8}$$

$$D_{m,i}^I = \mathrm{a}_i a_q G_{p,m,i}^{I,qp}\left(\left.\frac{\partial I_m(\mathrm{a}_i r_q)}{\partial r_q}\right|_{r=a_q}\frac{1}{I_m(\mathrm{a}_i a_q)} - \left.\frac{\partial K_m(\mathrm{a}_i r_q)}{\partial r_q}\right|_{r=a_q}\frac{1}{K_m(\mathrm{a}_i a_q)}\right) \tag{B9}$$

Here $R_{mn}^{III}, R_{mn}^{*III}$ are defined in the Appendix A (Eq. (A2)) and $G_{p,m,i}^{I,qp}$ is defined by Eqs. (2.35)–(2.37).

References

Abramowitz, M., Stegun, I.A., 1970. Handbook of mathematical functions. Dover Publications Inc, New York.

Aubault, A., Alves, M., Sarmento, A., Roddier, D., Peiffer, A., 2011. Modeling of an oscillating water column on the floating foundation windfloat. Offshore Arct. Eng. 5, 235–246.

Babarit, A., Borgarino, B., Ferrant, P., Clement, A., 2010. Assessment of the influence of the distance between two wave energy converters on energy production. IET Renew. Power Gener. 4, 592–601.

Babarit, A., 2013. On the park effect in arrays of oscillating wave energy converters. Renew. Energy 58, 68–78.

Black, J.L., Mei, C.C., Bray, M.C.G., 1971. Radiation and scattering of water waves by rigid bodies. J. Fluid Mech. 46, 151–164.

Borgarino, B., Babarit, A., Ferrant, P., 2012. Impact of wave interactions effects on energy absorption in large arrays of wave energy converters. Ocean Eng. 41, 79–88.

Bryden I., Linfoot B., 2010. Wave and current testing of an array of wave energy converters. In: Proceedings of the HYDRALAB III, 2010. Hannover.

Child, B., Venugopal, V., 2010. Optimal configurations of wave energy device arrays. In: Ocean Eng. 37, 1402–1417.

Child B., Cruz J., Livingstone M., 2011. The development of a tool for optimising arrays of wave energy converters. In: Proceedings of the Ninth European Wave and Tidal Energy Conference, EWTEC.

Cruz, J., 2008. Ocean Wave Energy. Springer, Berlin, Heidelberg, Germany.

Evans, D.V., 1982. Wave-power absorption by systems of oscillating surface pressure distributions. J. Fluid Mech. 114, 481–499.

Evans, D.V., Porter, R., 1996. Efficient calculation of hydrodynamic properties of O. W.C type devices. OMAE I (Part B), 123–132.

Falcao, A.F. de O., 2002. Wave power absorption by a periodic linear array of oscillating water columns. Ocean Eng. 29, 1163–1186.

Falcao, A.F. de O., 2010. Wave energy utilization: a review of the technologies. Renew. Sustain. Energy Rev. 14 (3), 899–918.

Falnes, J., McIver, P., 1985. Surface wave interactions with systems of oscillating bodies and pressure distributions. Appl. Ocean Res. 7, 225–234.

Falnes, J., 2002. Ocean Waves and Oscillating Systems. Cambridge University Press, Cambridge, U.K.

Folley, M., Babarit, A., Child, B., Forehand, D., O'Boyle, L., Silverthorne, K., Spinneken, J., Stratigaki, V., Troch, P., 2012. A review of numerical modelling of wave energy converter arrays. American Society of Mechanical Engineers, pp. 535–545, In: ASME 2012 31st International Conference on Ocean, Offshore and Arctic Engineering, 2012.

Garrett, C.J.R., 1970. Bottomless harbors. In: J. Fluid Mech. 43, 433–449.

Garrett, C.J.R., 1971. Wave forces on a circular dock. In: J. Fluid Mech. 46 (No. 1), 129–139.

Gomes, R.P.F., Henriques, J.C.C., Gato, L.M.C., Falcao, A.F. de O., 2012. Hydrodynamic optimization of an axisymmetric floating oscillating water column for wave energy conversion. Renew. Energy 44, 328–339.

Kagemoto, H., Yue, D.K.P., 1986. Interactions among multiple three-dimensional bodies in water waves: an exact algebric method. J. Fluid Mech. 166, 189–209.

Kokkinowrachos, K., Mavrakos, S.A., Asorakos, S., 1986. Behavior of vertical bodies of revolution in waves. Ocean Eng. 13 (6), 505–538.

Kokkinowrachos K., Thanos I., Zibell H.G., 1987. Hydrodynamic analysis of some wave energy conversion systems. In: Proceedings of the OCEANS'87 Conference. Halifax, Canada, p. 566–574.

Konispoliatis D.N., Mavrakos S.A., 2013. Hydrodynamic Interactions among multiple cylindrical OWC's devices restrained in regular waves. In: Proceedings of the 28th International Workshop on Water Waves and Floating Bodies (IWWWFB2013), L'Isle sur la Sorgue, France.

Martins–Rivas, H., Mei, C.C., 2009a. Wave power extraction from an oscillating water column along a straight coast. In: Ocean Eng. 36, 426–433.

Martins–Rivas, H., Mei, C.C., 2009b. Wave power extraction from an oscillating water column at the tip of a breakwater. In: J. Fluid Mech. 626, 395–414.

Mavrakos, S.A., 1985. Wave loads on a stationary floating bottomless cylinder with finite wall thickness. In: Appl. Ocean Res. 7 (No. 4), 213–224.

Mavrakos, S.A, Koumoutsakos, P., 1987. Hydrodynamic interaction among vertical axisymmetric bodies restrained in waves. In: Appl. Ocean Res. 9 (No. 3).

Mavrakos, S.A., 1988. Hydrodynamic coefficients for a thick-walled bottomless cylindrical body floating in water of finite depth. In: Ocean Eng. 15 (No 3), 213–229.

Mavrakos, S.A., 1991. Hydrodynamic coefficients for groups of interacting vertical axisymmetric bodies. In: Ocean Eng. 18 (5), 485–515..

Mavrakos, S.A., 1995. Users manual for the software HAMVAB. School of Naval Architecture and Marine Engineering, Laboratory for Floating Structures and Mooring Systems, Athens, Greece.

Mavrakos S.A., 1996. Diffraction loads on arrays of truncated hollow cylinders. In: Proceedings, 1st International Conference on Marine Industry (MARIND' 96). Varna Bulgaria, Vol. III, p. 91–105.

Mavrakos, S.A., McIver, P., 1997. Comparison of methods for computing hydrodynamic characteristics of array of wave power devices. Appl. Ocean Res. 19, 283–291.

Mavrakos, S.A., Katsaounis, G.M., 2010. Effects of floaters' hydrodynamics on the performance of tightly moored wave energy converters. IET Renew. Power Gener. 4 (Iss. 6), 531–544..

Mavrakos S.A., Konispoliatis D.N., 2012. Hydrodynamics of a free floating vertical axisymmetric oscillating water column device. In: Hindawi Publishing Corporations Journal of Applied Mathematics, Mathematical Modelling of Marine Structures, Vol. 2012; Article ID 142850.

McCormick, M.E., 1980. Ocean Wave Energy Conversion. Wiley, New York, N.Y.

McIver, P., 2005. Complex resonances in the water–wave problem for a floating structure. J. Fluid Mech. 536, 423–443.

Mei, C.C., 1983. The Applied Dynamics of Ocean Surface Waves. John Wiley, New York.

Miles, J., Gilbert, F., 1968. Scattering of gravity waves by a circular dock. J. Fluid Mech. 34 (No. 4), 783–793.

Nader, J.R., Zhu, S.P., Cooper, P., Steppenbelt, B., 2012. A finite element study of the efficiency of arrays of oscillating water column wave energy converters. Ocean Eng. 43, 72–81.

Nader, J.R., 2013. Interaction of ocean waves with oscillating water column wave energy convertors. University of Wollongong, Australia, PhD.

Nader, J.R., Zhu, S.P., Cooper, P., 2014. Hydrodynamic and energetic properties of a finite array of fixed oscillating water column wave energy converters. Ocean Eng., 88; , pp. 131–148.

Newman, J.N., 1977a. Marine Hydrodynamics. MIT Press, Cambridge, Massachusetts.

Newman, J.N., 1977b. The motions of a floating slender torus. J. Fluid Mech. 83, 721–735.

Nihous, G.C., 2012. Wave power extraction by arbitrary arrays of non-diffracting oscillating water columns. J. Ocean Eng. 51, 94–105.

Okhusu, M., 1974. Hydrodynamic forces on multiple cylinders in waves. University College London, London, In: Int. Symposium on the Dynamics of Marine Vehicles and structures in Waves.

Pinkster J.A., Oortmerssen G.Van., 1977. Computation of the first and second order wave forces on oscillating bodies in regular waves. In: Proceedings 2nd Int. Conf. on Numerical Ship Hydrodynamics, Berkeley.

Sarmento, A.J.N.A., Falcao, A.F. de O., 1985. Wave generation by an oscillating surface-pressure and its application in wave-energy extraction. J. Fluid Mech. 150, 467–485.

Sarmento, A.J.N.A., Gato, L.M.C., Falcao, A.F. de O., 1990. Turbine controlled wave energy absorption by oscillating water column devices. Ocean Eng. 17 (No. 5), 481–497.

Siddorn, P., Eatock Taylor, R., 2008. Diffraction and independent radiation by an array of floating cylinders. Ocean Eng., 35; , pp. 1289–1303.

Singh, J., Babarit, A., 2014. A fast approach coupling Boundary Element Method and plane wave approximation for wave interaction analysis in sparse arrays of wave energy converters. Ocean Eng., 85; , pp. 15–20.

Twersky, V., 1952. Multiple scattering of radiation by an arbitrary configuration of parallel cylinders. J. Acoust. Soc. Am. 24 (No.1).

Watson, G.N., 1966. A treatise on the theory of Bessel functions, (2nd Edn) Cambridge University Press, Cambridge.

Yeung, R.W., 1981. Added mass and damping of a vertical cylinder in finite–depth waters. Appl. Ocean Res. 3 (No. 3), 119–133.